Molecular dynamics simulations of Si etching in Cl- and Br-based plasmas: Cl+ and Br+ ion incidence in the presence of Cl and Br neutrals

Nobuya Nakazaki, Yoshinori Takao, Koji Eriguchi, and Kouichi Ono

Citation: Journal of Applied Physics **118**, 233304 (2015); doi: 10.1063/1.4937449
View online: http://dx.doi.org/10.1063/1.4937449
View Table of Contents: http://scitation.aip.org/content/aip/journal/jap/118/23?ver=pdfcov
Published by the AIP Publishing

Molecular dynamics simulations of Si etching in Cl- and Br-based plasmas: Cl^+ and Br^+ ion incidence in the presence of Cl and Br neutrals

Nobuya Nakazaki,[a] Yoshinori Takao,[b] Koji Eriguchi, and Kouichi Ono[c]
Department of Aeronautics and Astronautics, Graduate School of Engineering, Kyoto University, Kyoto-daigaku Katsura, Nishikyo-ku, Kyoto 615-8540, Japan

(Received 10 September 2015; accepted 26 November 2015; published online 18 December 2015)

Classical molecular dynamics (MD) simulations have been performed for Cl^+ and Br^+ ions incident on Si(100) surfaces with Cl and Br neutrals, respectively, to gain a better understanding of the ion-enhanced surface reaction kinetics during Si etching in Cl- and Br-based plasmas. The ions were incident normally on surfaces with translational energies in the range $E_i = 20$–500 eV, and low-energy neutrals of $E_n = 0.01$ eV were also incident normally thereon with the neutral-to-ion flux ratio in the range $\Gamma_n^0/\Gamma_i^0 = 0$–$100$, where an improved Stillinger–Weber potential form was employed for the interatomic potential concerned. The etch yields and thresholds presently simulated were in agreement with the experimental results previously reported for Si etching in Cl_2 and Br_2 plasmas as well as in Cl^+, Cl_2^+, and Br^+ beams, and the product stoichiometry simulated was consistent with that observed during Ar^+ beam incidence on Si in Cl_2. Moreover, the surface coverage of halogen atoms, halogenated layer thickness, surface stoichiometry, and depth profile of surface products simulated for $\Gamma_n^0/\Gamma_i^0 = 100$ were in excellent agreement with the observations depending on E_i reported for Si etching in Cl_2 plasmas. The MD also indicated that the yield, coverage, and surface layer thickness are smaller in Si/Br than in Si/Cl system, while the percentage of higher halogenated species in product and surface stoichiometries is larger in Si/Br. The MD further indicated that in both systems, the translational energy distributions of products and halogen adsorbates desorbed from surfaces are approximated by two Maxwellians of temperature $T_1 \approx 2500$ K and $T_2 \approx 7000$–$40\,000$ K. These energy distributions are discussed in terms of the desorption or evaporation from hot spots formed through chemically enhanced physical sputtering and physically enhanced chemical sputtering, which have so far been speculated to both occur in the ion-enhanced surface reaction kinetics of plasma etching. © *2015 AIP Publishing LLC*.
[http://dx.doi.org/10.1063/1.4937449]

I. INTRODUCTION

Plasma etching is still and will continue to be a key technology for manufacturing nanometer-scale microelectronic devices.[1–3] As the device dimensions continue to be scaled down to much less than several 10 nm,[4] increasingly strict requirements are being imposed on plasma etching technology, including the precise control of profile, critical dimension (CD), roughness, and their microscopic uniformity (or aspect-ratio dependence), along with that of etch rate, selectivity, and damage. The atomic- or nanometer-scale control of Si etching in Cl- and Br-based plasmas is indispensable for the recent fabrication of transistor gate and fin structures and shallow trench isolation.[5,6] In gate and fin fabrications, the CD loss/gain on the order of 1 nm is required for sidewall profiles,[5,7] and the roughness on sidewalls and bottom surfaces of the feature is required to be less than 1 nm,[6,8] to suppress the variability in transistor performance. To meet these requirements, a deeper understanding of plasma-surface interactions underlying the processing is increasingly important on the atomic scale. A number of experiments have been concerned with Si etching in Cl_2-, Br_2-, and HBr-containing plasmas to reveal the surface reaction kinetics during etching such as ion-enhanced etching and passivation layer formation through investigating the etch yield and threshold,[9,10] and the microscopic surface structures of reaction[11–14] and passivation[15–18] layers, e.g., their thickness, coverage, and depth profile of halogen and other atoms adsorbed, and stoichiometry and depth profile of reaction products contained therein. However, the surface reaction kinetics during plasma etching are not yet fully understood owing to the plasma environments of enormous complexity.

Classical molecular dynamics (MD) simulations have been developed in the last two decades to clarify the surface reaction kinetics on the atomic scale during plasma etching of Si, SiO_2, and low dielectric constant (low-k) films with F- and Cl-based chemistries, giving fundamental etching characteristics such as etch yield, threshold, product stoichiometry, and microscopic surface structures.[19] In particular, a number of MD studies have been concerned with Cl^+ and/or Cl_2^+ ion impacts onto Si surfaces, using the interatomic potential models of Stillinger–Weber (SW)[20–29] and Tersoff–Brenner (TB)[30–32] types. We have also developed MD simulations for Si/Br and Si/HBr as well as Si/Cl systems,[33–39] along with an improved SW interatomic potential

[a]Electronic mail: nakazaki.nobuya.58x@st.kyoto-u.ac.jp
[b]Present address: Division of Systems Research, Faculty of Engineering, Yokohama National University, Tokiwadai, Hodogaya-ku, Yokohama 240-8501, Japan.
[c]Electronic mail: ono@kuaero.kyoto-u.ac.jp

model for Si/halogen interactions,[37–39] because of a poor understanding of plasma-surface interactions for Br-based plasma etching of Si in experiments as well as simulations. Moreover, we have recently developed MD simulations of incidence of ionized etch products $SiCl_x^+$ ($x=0$–4) as well as feed gas ions Cl_x^+ ($x=1$, 2) during Si etching in Cl-based plasmas, revealing the etch fundamentals of depositive $SiCl_x^+$ ($x=0$–2) ions as well as those of reactive $SiCl_x^+$ ($x=3$, 4) and Cl_x^+ ($x=1$, 2) ions;[40] in practice, the experiments showed that $SiCl_x^+$ ions might play a crucial role in the evolution of surface roughness during plasma etching of Si in Cl-based plasmas.[41,42] However, most of these MD studies have been concerned with incidence of energetic ions, and few studies have so far been concerned with ion incidence in the presence of incoming low-energy neutrals, which is generally appreciated to occur in real plasma etching environments.[43] Humbird and Graves reported MD simulations of spontaneous etching of Si by Cl[30,31] as well as F[30,31,44] atoms, to give their surface coverage, depth profile, etch reaction probability, and product stoichiometry, where the TB type potential was employed, and thermal neutrals were incident on Si surfaces amorphized by energetic Ar^+ ion impacts. Tinck *et al*. have recently reported MD simulations of cryogenic etching of Si by SiF_x ($x=0$–4) and F_x ($x=1$, 2) neutrals with thermal velocities and the corresponding energetic ions, using a combination of a Tersoff interatomic potential and a long-range Lennard–Jones type van der Waals interaction potential;[45] they gave sticking probabilities, thermal desorption rates, surface diffusion speeds, and sputter yields of the species concerned on Si and on SiF_x ($x=1$–3) surfaces, both at cryogenic and near room temperature.

This paper presents MD simulations of Cl^+ and Br^+ ions normally incident on Si(100) surfaces in the presence of incoming low-energy Cl and Br atoms, respectively, with emphasis being placed on a better understanding of the ion-enhanced surface reaction kinetics during Si etching in Cl- and Br-based plasmas. The ion incident energy concerned was in the range $E_i=20$–500 eV, where the incoming neutral-to-ion flux ratio was taken to be in the range $\Gamma_n^0/\Gamma_i^0=0$–100; preliminary results for Si/Cl system with $E_i=100$ eV and $\Gamma_n^0/\Gamma_i^0=100$ were reported in our previous paper.[34] Section II describes the simulation model and numerical procedures used in this study. Numerical results are then given in Sec. III for the etch fundamentals such as etch yield and threshold, product stoichiometry, desorption yield of halogen adsorbates, energy and angular distributions of products and adsorbates desorbed, and microscopic structures of surface reaction layers (thickness, coverage, stoichiometry, and depth profile). A comparison is made with the experiments of Si etching in Cl_2 and Br_2 plasmas as well as those in Cl^+, Cl_2^+, and Br^+ beams previously reported, to verify these MD simulations. Finally, Sec. IV summarizes the conclusions of this paper.

II. SIMULATION MODEL

Figure 1(a) shows a schematic of the classical MD simulation for etching that is similar to that in our previous

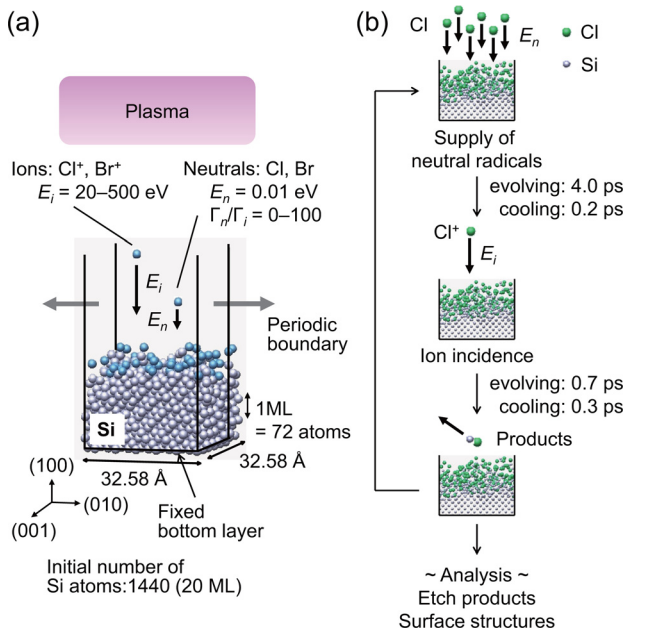

FIG. 1. (a) Schematic and (b) calculation scheme of the classical MD simulation for plasma etching with exposure of energetic ions and low-energy neutrals, where every after injection of an energetic ion, a set of neutrals are supplied onto the surface. The ions of interest are Cl^+ and Br^+ with translational energies in the range $E_i=20-500$ eV (unless otherwise stated), being normally incident on Si(100) surfaces; Cl and Br neutrals of translational energy $E_n=0.01$ eV are also incident normally thereon with the neutral-ion-flux ratio in the range $\Gamma_n^0/\Gamma_i^0=0-100$. Substrate or target Si atoms are placed in the simulation cell, which has a square of 32.58 Å on one side and contains target atoms of 20 monolayer (ML) or 1440 Si atoms in a depth of 26.0 Å. Note that an ML contains 72 Si atoms ($=6.78\times10^{14}$ atoms/cm^2).

studies.[33–40] Briefly, substrate or target Si atoms are placed in the simulation cell, initially having a structure of a diamond lattice the top surface of which corresponds to the Si(100) plane. The Si(100) surface concerned is a square 32.58 Å on one side (with an area of 1061 Å^2), where a monolayer (ML) contains 72 Si atoms (or 6.78×10^{14} atoms/cm^2). The simulation cell initially contains target atoms of 20 ML (or 1440 Si atoms) in a depth of 26.0 Å. Target atoms in the bottom two layers are fixed during the simulation, while periodic boundaries are imposed in the horizontal direction. Energetic Cl^+ and Br^+ ions are injected vertically ($\theta_i=0°$) toward the surface from randomly selected horizontal locations above the target with translational energies in the range $E_i=20$–500 eV, unless otherwise stated. It is further noted that while energetic species are often referred to as "ions," they are assumed to be neutralized owing to the Auger process just before impact and then interact with the surface as neutrals.[46]

To simulate plasma etching environments with simultaneous exposure of energetic ions and neutral reactants, low-energy Cl and Br atoms are supplied normally ($\theta_n=0°$) onto the surface also from random horizontal locations above the target prior to every ion impact. The number of neutrals supplied per ion impact corresponds to the incoming neutral-to-ion flux ratio in plasma environments, which is taken to be in the range $\Gamma_n^0/\Gamma_i^0=0$–100; in practice, $\Gamma_n^0/\Gamma_i^0=0$ simulates the etching by energetic ions only, and $\Gamma_n^0/\Gamma_i^0=100$ the etching by typical high-density plasmas such as inductively coupled[41,42] and electron cyclotron resonance[47–50] plasmas. The translational energy of neutrals is taken to be typically

$E_n = 0.01$ eV, which would be low enough not to etch Si but to stick on the surface.

The species concerned are ^{28}Si, ^{35}Cl, and ^{80}Br with the respective atomic masses of 28.0855, 35.4529, and 79.9035 g/mol. The interatomic potential presently employed has a form of the SW potential function for covalent bonds:[51–54] $\Phi = \sum_{i<j} v_2(i,j) + \sum_{i<j<k} v_3(i,j,k)$, where the total potential energy is expressed by the summation of the two- and three-body potential functions. In practice, the repulsive interaction is overestimated in the original SW model, when a halogen atom is surrounded by more than three Si atoms, and/or when a high-energy halogen penetrates deeper into substrates. Thus we employ an improved potential form of the SW model,[37,38] which involves a correction term for the three-body potential function, to overcome this disadvantage and to predict surface reaction kinetics more accurately. A known parameter set is used for the interatomic potential of the Si/Cl system,[20] while a parameter set developed by the authors is used for that of the Si/Br system.[35]

Figure 1(b) shows a calculation scheme of the MD simulation for plasma etching that is in a sense similar to the so-called digital or atomic layer etching of Si consisting of a repetition of Ar^+ ion incidence followed by that of neutral reactants.[55–57] After every injection of an energetic ion (Cl^+, Br^+), we let the system evolve for 0.7 ps with the total energy being constant and then artificially cool the system for 0.3 ps down to the initial temperature (300 K) of target atoms, where the temperature is taken to be the mean kinetic energy over the target atoms contained in the simulation cell. The artificial cooling of the system is made by employing the Berendsen heat removal scheme[58] with a coupling constant of 2.0×10^{14} s^{-1}.[23,26,29] Similarly, after every introduction of a set of low-energy neutrals (Cl, Br), we let the system evolve for 4.0 ps and then cool it for 0.2 ps. In addition, we sometimes add a layer of Si atoms at the bottom of the simulation cell to maintain the number of target atoms above ~20 ML therein during etching. The etch fundamentals, such as etch yield and threshold, product stoichiometry, desorption yield of halogen adsorbates, energy and angular distributions of products and adsorbates desorbed, and microscopic structures of surface reaction layers (thickness, coverage, stoichiometry, and depth profile), are analyzed after every ion impact; then they are averaged over 1000 ion impacts after the etching characteristics and surface structures have become statistically stable, unless otherwise stated.

It should be noted that in high-density plasma etching environments, the ion flux onto substrate surfaces is often <10 mA/cm^2 (or $\Gamma_i^0 < 6.2 \times 10^{16}$ cm^{-2}s^{-1}),[41,42,47–50] in which energetic ions impact the surface presently concerned at most approximately once every 10^{-4} s, and so individual ion impacts may be virtually assumed to be temporally isolated events. On the other hand, the MD simulations are limited to times of the order of 10^{-12} s, and so longer time-scale events such as thermal diffusion, reaction, and desorption (that are undoubtedly occurring in surface layers after ion impact) are not likely to occur intrinsically during relatively short times of the simulation. We took the simulation time of 1 ps (evolving and cooling times of 0.7 and 0.3 ps, respectively, as mentioned in the preceding text) based on the transit time for a "shock wave" to traverse the distance from the top surface to the fixed bottom layer of the simulation cell and back,[23,26,29] which is slightly less than that of 1–2 ps generally taken in other MD studies.[19] No significant change was confirmed in the etching characteristics and surface structures obtained for varying the evolving and cooling times in the range 0.7–2.8 and 0.3–2.1 ps, respectively (or the simulation time in the range 1–5 ps).

III. RESULTS AND DISCUSSION

A. Overview

Figure 2 shows typical side views of the Si(100) surface, together with the depth profiles of Ha and Si atoms therein, simulated for Si/Ha (Ha = Cl, Br) systems with different ion energies of $E_i = 50$, 100, and 300 eV and neutral-to-ion flux ratios of $\Gamma_n^0/\Gamma_i^0 = 0$ and 100. The side views shown are typical snapshots of the surface taken after 2000 ion impacts and the following evolving-cooling procedure, while the depth profiles are averages over more than ten hundred snapshots of the surface thereafter. Note that the depth profile of interest here is the vertical distribution of the laterally averaged concentration of the respective atoms, and that the depth of zero in the figure is taken to be the position giving the mean (volume averaged) value of the concentration of Ha atoms contained. The results indicate that in both systems, the thickness of surface $SiHa_x$ layers increases (or the distribution of Ha atoms contained therein broadens) with increasing E_i, owing to the increased penetration depth of incident ions into substrates. Moreover, at a given E_i, the $SiHa_x$ layer thickness tends to be slightly decreased for increased Γ_n^0/Γ_i^0, owing to the enhanced desorption of surface reaction products or Si_xHa_y compounds therefrom; correspondingly, the concentration of Ha atoms in the upper half layers tends to be increased for increased Γ_n^0/Γ_i^0, being comparable to or higher than that of Si atoms therein, owing to the increased supply of neutrals onto the surface. A comparison between Si/Cl and Si/Br systems indicates that Br atoms penetrate shallower into substrates or the thickness of surface $SiHa_x$ layers is smaller in Si/Br, which is attributed to the larger atomic radius of Br; in effect, the equilibrium distance (or the interatomic distance at the minimum) of the two-body potential function is known to be $r_0 = 2.06$ Å for Si−Cl,[20,35] 2.32 Å for Si−Br,[35] and 2.35 Å for Si−Si.[20,35] In addition, in Si/Br, the concentration of Br atoms in the upper half layers is comparable to or higher than that of Si atoms therein even for $\Gamma_n^0/\Gamma_i^0 = 0$ at lower $E_i = 50$ and 100 eV.

Figure 3 shows the Si yield Y_{Si} per ion impact, halogen yield Y_{Ha} per ion impact, surface coverage of Ha atoms adsorbed or the total number of Ha atoms contained per unit area in surface $SiHa_x$ layers, and their thickness as a function of ion impact, simulated for Si/Ha (Ha = Cl, Br) systems with an ion energy of $E_i = 100$ eV and different neutral-to-ion flux ratios of $\Gamma_n^0/\Gamma_i^0 = 0$ and 100. These are instantaneous values after every ion impact. Here the Si yield Y_{Si} (per ion) or the etch yield is defined as the total number of Si atoms desorbed from substrate surfaces per ion impact, and

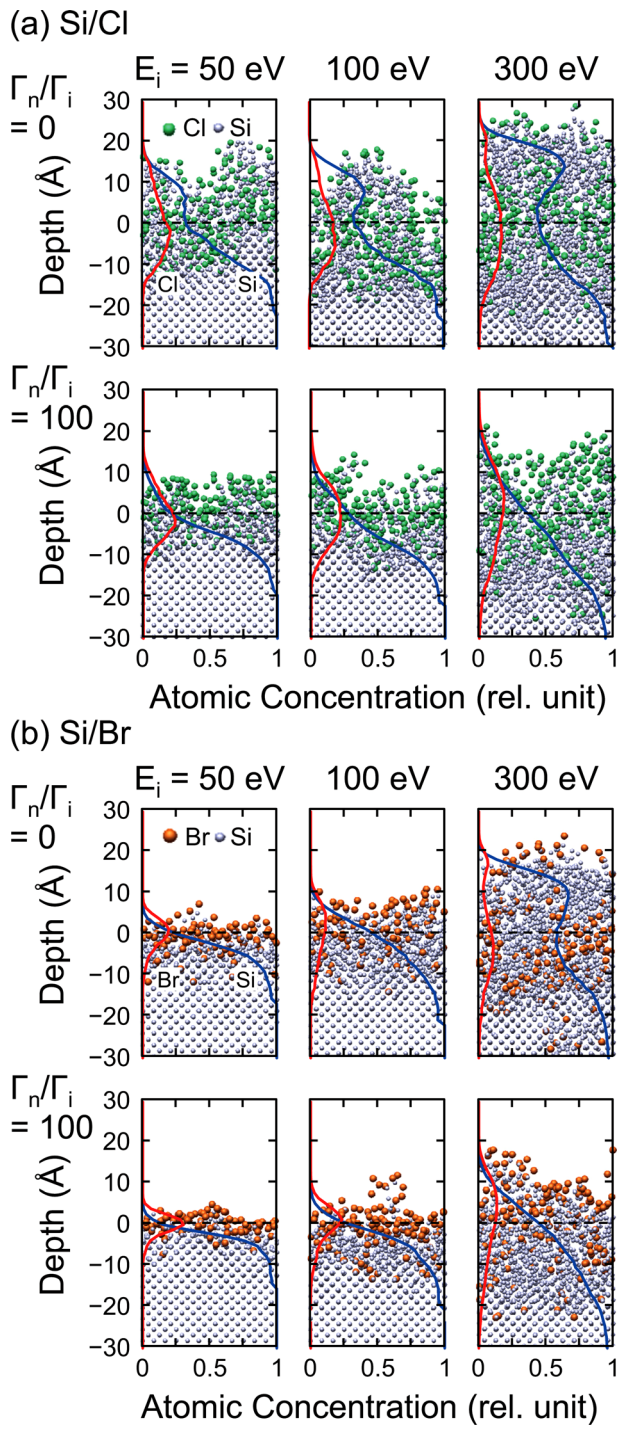

FIG. 2. Side views of the Si(100) surface, together with the depth profiles of Ha and Si atoms therein (Ha = Cl, Br), simulated for (a) Si/Cl and (b) Si/Br systems with different ion energies of $E_i = 50$, 100, and 300 eV and neutral-to-ion flux ratios of $\Gamma_n^0/\Gamma_i^0 = 0$ and 100. The side views shown are typical snapshots of the surface taken after 2000 ion impacts and the following evolving-cooling procedure, while the depth profiles are averages over more than ten hundred snapshots of the surface thereafter. Note that the depth profile of interest here is the vertical distribution of the laterally averaged concentration of the respective atoms, and that the depth of zero in the figure is taken to be the position giving the mean (volume averaged) value of the concentration of Ha atoms contained.

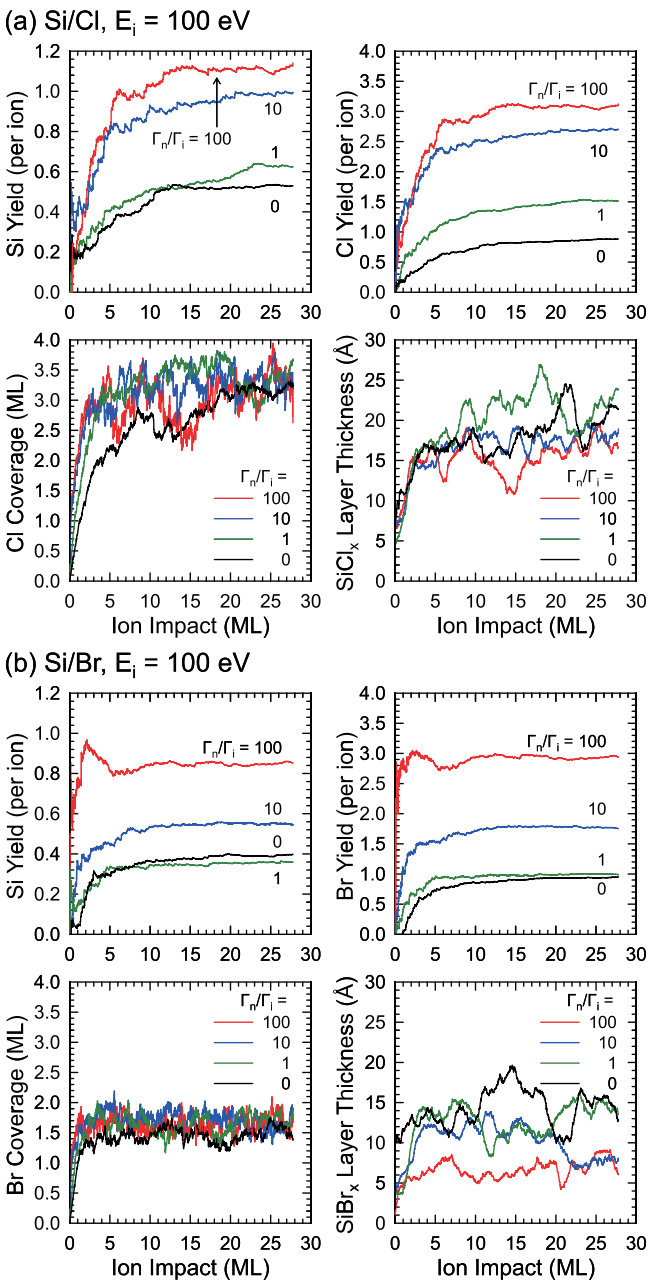

FIG. 3. Si yield Y_{Si} per ion impact, halogen yield Y_{Ha} per ion impact, surface coverage of Ha atoms adsorbed or the total number of Ha atoms contained per unit area in surface $SiHa_x$ layers (Ha = Cl, Br), and their thickness (FWHM) as a function of ion impact, simulated for (a) Si/Cl and (b) Si/Br systems with an ion energy of $E_i = 100$ eV and different neutral-to-ion flux ratios of $\Gamma_n^0/\Gamma_i^0 = 0$ and 100. These are instantaneous values after every ion impact. Here the Si yield Y_{Si} (per ion) or the etch yield is defined as the total number of Si atoms desorbed from substrate surfaces per ion impact, and the halogen yield Y_{Ha} (per ion) as the total number of Ha atoms desorbed from surfaces per ion impact (including the contribution of incident Ha^+ ion reflected or scattered from the surface on incidence); in practice, the yields Y_{Si} and Y_{Ha} are counted during the evolving-cooling period following ion impact. Note that 1 ML corresponds to the areal density of 6.78×10^{14} atoms/cm^2 (integrated throughout the layer) for coverage, and to 72 incident ions for ion impact.

the halogen yield Y_{Ha} (per ion) as that of Ha atoms desorbed from surfaces per ion impact (including the contribution of incident Ha^+ ion reflected or scattered from the surface on incidence); in practice, the yields Y_{Si} and Y_{Ha} are counted during the evolving-cooling period following ion impact. Note that 1 ML corresponds to the areal density of 6.78×10^{14} atoms/cm^2 (integrated throughout the layer) for coverage, and to 72 incident ions for ion impact; then, 27.77 ML or 2000 ion impacts onto the surface presently

concerned correspond to the processing time of 1.88 s in typical high-density plasma etching environments with $\Gamma_i^0 = 1.0 \times 10^{16}\,\mathrm{cm^{-2}s^{-1}}$.[41,42,47–50] In addition, the $SiHa_x$ layer thickness is defined as the full width at half maximum (FWHM) of the depth profile of Ha atoms therein.

The results indicate that in both systems, the yields Y_{Si} and Y_{Ha} increase and then reach quasi-steady state at the initial stage of ion impact up to about several ML, along with the Ha coverage and $SiHa_x$ layer thickness; moreover, at steady state, the Y_{Si} and Y_{Ha} values are increased and the $SiHa_x$ layer thickness is slightly decreased for increased Γ_n^0/Γ_i^0, while the Ha coverage remains almost unchanged over the Γ_n^0/Γ_i^0 range investigated. A comparison between Si/Cl and Si/Br systems indicates that the Si/Br system evolves to reach quasi-steady state sooner after the start of ion impact and that at steady state, the yields Y_{Si} and Y_{Ha}, Ha coverage, and $SiHa_x$ layer thickness tend to be smaller in Si/Br. It is further noted that similar evolutions were also observed for different $E_i = 20$–500 eV in both systems, although more ion impacts tend to be required for the system to reach quasi-steady state at increased E_i.

B. Etch yield and product stoichiometry

Figure 4 shows the Si yields Y_{Si} per ion impact, together with the stoichiometry of Si-containing product species Si_xHa_y ($x \geq 1$, $y \geq 0$) desorbed, simulated for Si/Ha (Ha = Cl, Br) systems with different ion energies of $E_i = 20$–500 eV and neutral-to-ion flux ratios of $\Gamma_n^0/\Gamma_i^0 = 0$–100. The results indicate that in both systems, the yield Y_{Si} increases with increasing E_i, along with the percentage of elemental Si and low-halogenated Si_xHa_y species; moreover, at a given E_i, the yield Y_{Si} is increased for increased Γ_n^0/Γ_i^0 along with the percentage of higher-halogenated Si_xHa_y species. In Si/Cl system, e.g., for $\Gamma_n^0/\Gamma_i^0 = 0$, the predominant product species is SiCl and then $SiCl_2$ at $E_i = 50$ eV, while it is elemental Si and then SiCl at $E_i = 500$ eV; and for $\Gamma_n^0/\Gamma_i^0 = 100$, the predominant species is $SiCl_2$ and then $SiCl_3$ at $E_i = 50$ eV, while it is SiCl and then $SiCl_2$ at $E_i = 500$ eV. The E_i and Γ_n^0/Γ_i^0 dependences of the yield and product stoichiometry presently simulated are consistent with the experiments of Ar^+ beam incidence on Si in Cl_2[59–64] and Cl_2/Cl[65,66] previously reported, being ascribed to the increased effects of physical sputtering or the decreased chemical effects in sputtering with increasing E_i and to the increased surface halogenation/chlorination for increased Γ_n^0/Γ_i^0. The yield of fully chlorinated species $SiCl_4$ is extremely small with a percentage $< 0.05\%$ of the total for any E_i and Γ_n^0/Γ_i^0.

A comparison between Si/Cl and Si/Br systems indicates that the yield Y_{Si} is smaller in Si/Br, owing to the less chemical reactivity of Br on Si, as has been observed in Si etching experiments with Cl^+ and Br^+ beams,[67,68] Cl_2 and Br_2 plasma beams,[9,10] and high-temperature Cl_2 and Br_2 gases.[69,70] Moreover, higher-halogenated Si_xHa_y species tend to be formed and desorbed in Si/Br, where fully brominated species $SiBr_4$ occurs with a percentage $< 5\%$ of the total for any E_i and Γ_n^0/Γ_i^0. This is attributed partly to higher

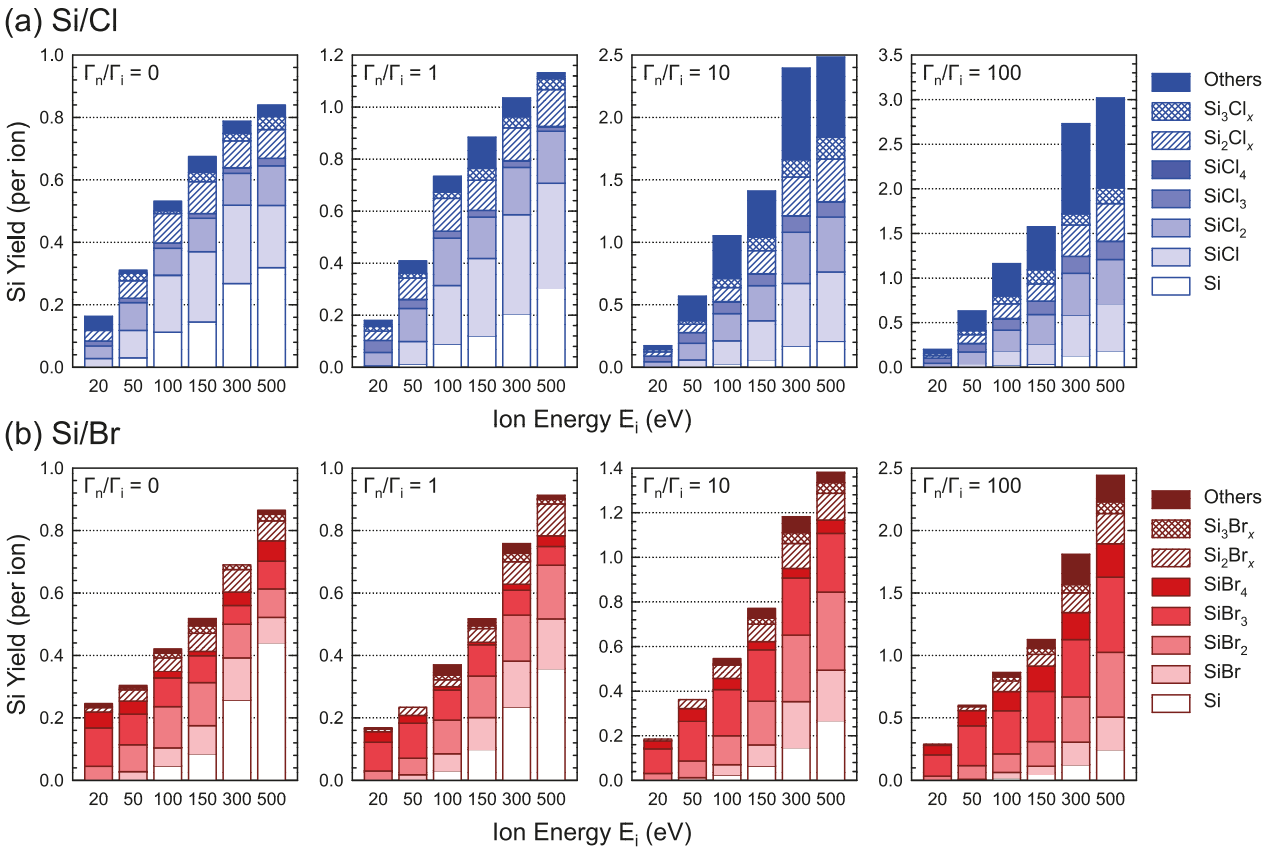

FIG. 4. Si yields Y_{Si} per ion impact, together with the stoichiometry of Si-containing product species Si_xHa_y ($x \geq 1$, $y \geq 0$) desorbed (Ha = Cl, Br), simulated for (a) Si/Cl and (b) Si/Br systems with different ion energies of $E_i = 20$–500 eV and neutral-to-ion flux ratios of $\Gamma_n^0/\Gamma_i^0 = 0$–100. Note that "Others" in the legend indicates Si_xHa_y species ($x \geq 4$, $y \geq 0$).

concentrations of Ha atoms in the near-surface region of thinner $SiHa_x$ layers in Si/Br system (as seen in Fig. 2) and thus to higher percentages of high-halogenated surface products such as $SiHa_3$ and $SiHa_4$ therein (as will be seen later in Figs. 9 and 10).

Figure 5 shows the Si yield Y_{Si} per ion impact as a function of the square root of the ion incident energy, $\sqrt{E_i}$, simulated for Si/Ha (Ha = Cl, Br) systems with different ion energies of $E_i = 10$–500 eV and neutral-to-ion flux ratios of $\Gamma_n^0/\Gamma_i^0 = 0$–100. Also shown are the MD simulations of Cl^+ incidence on Si performed by Hanson *et al.*[23] using the SW potential and by Gou *et al.*[32] using the TB potential, along with the experiments for Si/Cl and Si/Br systems performed by Tachi and Okudaira[67] using Cl^+ and Br^+ beams, by Balooch *et al.*[64] using Cl_2^+ beams (including $\lesssim$30% Cl^+), by Chang and Sawin[65] using Cl^+ beams with and without neutral Cl, and by Vitale *et al.*[9] and Jin *et al.*[10] using Cl_2 and Br_2 plasma beams. Our MD simulations for Si/Cl system using the improved SW potential are in agreement with these MD and experimental data previously reported; in particular, the yields Y_{Si} for Si/Cl obtained with $\Gamma_n^0/\Gamma_i^0 = 0$ fit rather well with the MD simulations of Gou *et al.*[32] and the beam experiments of Chang and Sawin,[65] while those with $\Gamma_n^0/\Gamma_i^0 = 100$ are roughly two times smaller than the beam-plus-neutral experiments of Chang and Sawin ($\Gamma_n^0/\Gamma_i^0 \approx$ 100–300)[65] and the plasma beam experiments of Vitale *et al.* ($\Gamma_n^0/\Gamma_i^0 \approx$ 900–4400)[9] and Jin *et al.*[10]

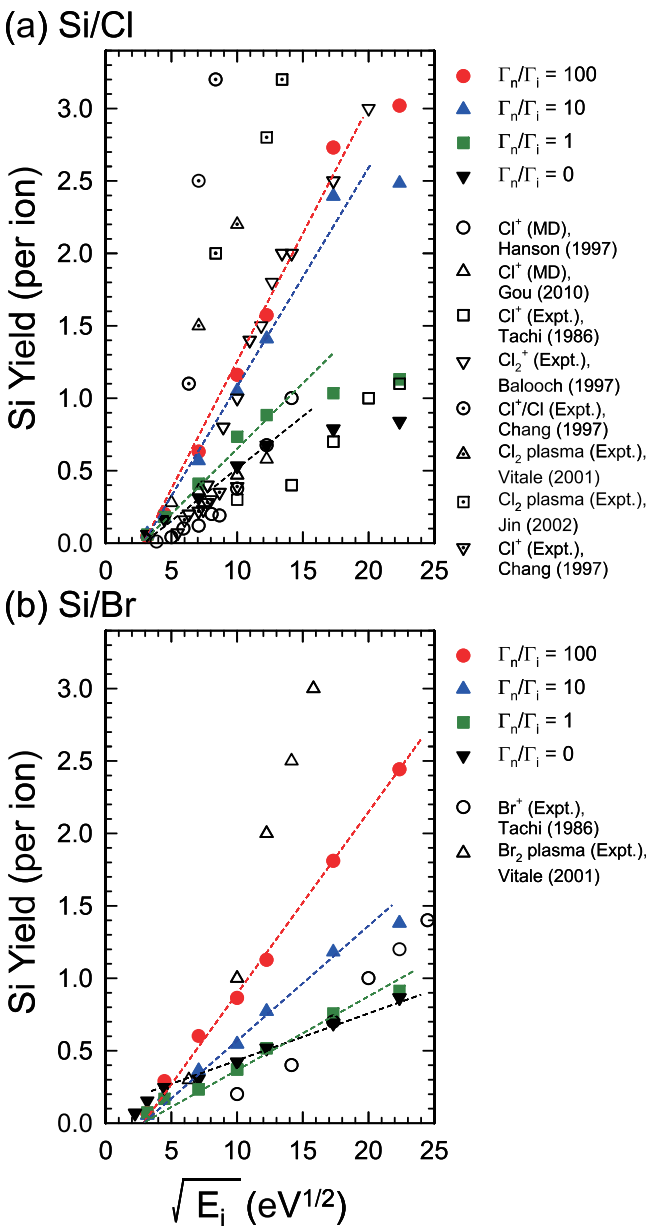

FIG. 5. Si yield Y_{Si} per ion impact as a function of the square root of the ion incident energy, $\sqrt{E_i}$, simulated for (a) Si/Cl and (b) Si/Br systems with different ion energies of $E_i = 10-500$ eV and neutral-to-ion flux ratios of $\Gamma_n^0/\Gamma_i^0 = 0-100$. Also shown are the MD simulations of Cl^+ incidence on Si performed by Hanson *et al.*[23] using the SW potential and by Gou *et al.*[32] using the TB potential, along with the experiments for Si/Cl and Si/Br systems performed by Tachi and Okudaira[67] using Cl^+ and Br^+ beams, by Balooch *et al.*[64] using Cl_2^+ beams (including $\lesssim$30% Cl^+), by Chang and Sawin[65] using Cl^+ beams with and without neutral Cl, and by Vitale *et al.*[9] and Jin *et al.*[10] using Cl_2 and Br_2 plasma beams.

The present MD results indicate that in both systems, the yield Y_{Si} increases with increasing E_i and Γ_n^0/Γ_i^0; in more detail, for any Γ_n^0/Γ_i^0, the yield Y_{Si} is approximately proportional to $\sqrt{E_i}$, $Y_{Si} = A(E_i^{1/2} - E_{th}^{1/2})$, where A is a proportional constant or scaling factor, and E_{th} is the threshold energy concerned. The liner dependence of the yield Y_{Si} on $\sqrt{E_i}$ reflects the universal energy dependence of the yield for ion bombardment-induced etch processes such as physical sputtering and ion-enhanced etching,[64,65,71] implying that the sputtering or etching is limited by the momentum transfer from energetic ions to substrate atoms through the collision-cascade mechanism. The constant A is larger for higher flux ratios Γ_n^0/Γ_i^0. In Si/Cl system, the yield Y_{Si} at a given E_i (or the constant A) tends to be saturated for increased $\Gamma_n^0/\Gamma_i^0 > 10$; this implies that the system is limited by the availability of neutral reactants on the surface (neutral flux limited) for low $\Gamma_n^0/\Gamma_i^0 < 10$, while it is saturated with neutrals (ion flux limited) for higher Γ_n^0/Γ_i^0, as has been observed in Si etching experiments using Ar^+ beams with Cl_2[59–64] and Cl_2/Cl[65,66] as well as Cl^+ beams with Cl_2/Cl.[65] The threshold for Si/Cl is estimated to be $E_{th} \approx 9$ eV almost independently of Γ_n^0/Γ_i^0, by extrapolating the Y_{Si} to zero, being in agreement with the previous Si etching experiments using Cl^+ beams with Cl_2/Cl[65] and Cl_2 plasma beams.[9]

It is further noted that for any Γ_n^0/Γ_i^0 in Si/Cl system, the curve of Y_{Si} versus $\sqrt{E_i}$ tends to exhibit a transition point at around $E_i \approx$ 150–300 eV (increased for increased Γ_n^0/Γ_i^0), above which the Y_{Si} increases more slowly with increasing E_i, although it remains nearly proportional to $\sqrt{E_i}$; in practice, the slope or proportional constant A of the curve above the point is estimated to be decreased significantly by about a factor of more than 3–5, implying some change in reaction kinetics on surfaces being etched at increased E_i. Such a transition point has so far been observed in the Cl^+ and Br^+ beam experiments of Si etching (at $E_i \approx$ 500 eV);[67,68] however, the mechanisms concerned are not understood at present. In some cases, the energy dependence $Y_{Si} \propto \sqrt{E_i}$ may not be universal, requiring the constant A depending on E_i and/or some other fitting curves such as $Y_{Si} = A(E_i^b - E_{th}^b)$ with $b \neq 1/2$.[38]

A comparison between Si/Cl and Si/Br systems indicates that although similar trends occur in Si/Br, there are some other differences between them, in addition to smaller

Si yields Y_{Si} in Si/Br, as mentioned in the preceding text with respect to Fig. 4. In practice, for $\Gamma_n^0/\Gamma_i^0 \geq 1$ (with incoming neutrals) in Si/Br system, the yield Y_{Si} exhibits an almost linear increase with $\sqrt{E_i}$ over the E_i range investigated (there is no transition point); and the yield Y_{Si} at a given E_i (or the constant A) is increased for increased flux ratios Γ_n^0/Γ_i^0 without saturation, implying that the system is limited by the availability of neutral reactants on the surface (neutral flux limited) over the Γ_n^0/Γ_i^0 range concerned, probably owing to the less chemical reactivity of Br on Si; moreover, the threshold is estimated to be $E_{th} \approx 4$ eV almost independently of Γ_n^0/Γ_i^0. On the other hand, for $\Gamma_n^0/\Gamma_i^0 = 0$ (without neutrals) in Si/Br, the curve of Y_{Si} versus $\sqrt{E_i}$ appears to exhibit a transition point at around $E_i \approx 20$ eV, decreasing more sharply than $\sqrt{E_i}$ with decreasing E_i at low $E_i < 20$ eV to give also the threshold $E_{th} \approx 4$ eV.

It should be noted that the threshold $E_{th} \approx 4$ eV thus estimated for Si/Br system is much lower than the $E_{th} \approx 40$ eV obtained from the extrapolation of the experimental data for Br^+ beam[67] and Br_2 plasma beam ($\Gamma_n^0/\Gamma_i^0 \approx$ 4000–8000)[9] etching of Si; correspondingly, the slopes or constants A of the Y_{Si} versus $\sqrt{E_i}$ curves for Si/Br tend to be relatively small as compared to those obtained from the fitting of the data of beam and plasma experiments.[9,67] These suggest that the reactivity of Br on Si at low E_i (<several tens of eV) may be slightly large in our MD simulations for Si/Br system, or there may still remain some overestimation of the repulsive interaction in the improved SW potential for Si/Br;[35,37] this is also inferred from the Γ_n^0/Γ_i^0 dependence of the yield Y_{Si} at a given E_i in Si/Br [as in Fig. 4(b)], where the Y_{Si} at $E_i = 20$ eV is lower for $\Gamma_n^0/\Gamma_i^0 = 1$ and 10 than for $\Gamma_n^0/\Gamma_i^0 = 0$, and the Y_{Si} at $E_i = 50$ eV is also lower for $\Gamma_n^0/\Gamma_i^0 = 1$ than for $\Gamma_n^0/\Gamma_i^0 = 0$.

C. Desorption yield of halogen adsorbates

Figure 6 shows the halogen yields Y_{Ha} per ion impact, together with the stoichiometry of Ha-containing species Ha_x ($x = 1, 2$) and Si_xHa_y ($x \geq 1$, $y \geq 1$) desorbed, simulated for Si/Ha (Ha = Cl, Br) systems with different ion energies of E_i = 20–500 eV and neutral-to-ion flux ratios of Γ_n^0/Γ_i^0 = 0–100. The yield or stoichiometry concerned includes the contribution of incident Ha^+ ion reflected from the surface on incidence as well as that of adsorbates and surface reaction products desorbed: $Y_{Ha} = R_{Ha^+} + \sum_{x=1,2} xY(Ha_x) + \sum_{x\geq1, y\geq1} yY(Si_xHa_y)$, where R_{Ha^+} is the reflection probability for incident Ha^+ ions, the latter $Y_{ha} = \sum_{x=1,2} xY(Ha_x)$ and $Y_{ha/Si} = \sum_{x\geq1, y\geq1} y Y(Si_xHa_y)$ are the ion-induced desorption yields for adsorbates Ha_x and reaction products Si_xHa_y, respectively, and the Si yield as in Figs. 3–5 is given by $Y_{Si} = \sum_{x\geq1, y\geq0} xY(Si_xHa_y)$. The results indicate that for $\Gamma_n^0/\Gamma_i^0 = 0$ in both systems, the Ha yield remains almost unchanged at unity ($Y_{Ha} \approx 1$) for varying E_i because of the steady state achieved under Ha^+ ion incidence without incoming Ha neutrals; on the other hand, for $\Gamma_n^0/\Gamma_i^0 \geq 1$, it is assumed to be $Y_{Ha} > 1$ at steady state because the total

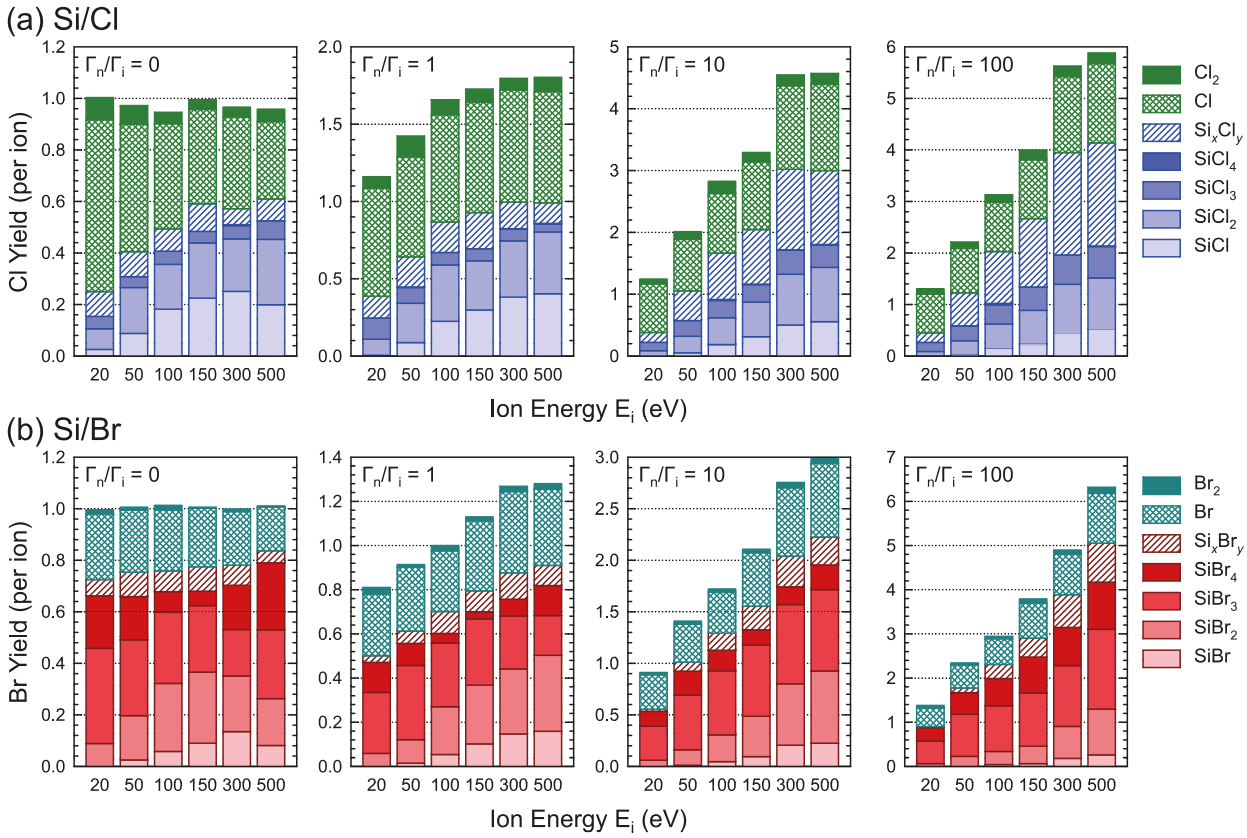

FIG. 6. Halogen yields Y_{Ha} per ion impact, together with the stoichiometry of Ha-containing species Ha_x ($x = 1, 2$) and Si_xHa_y ($x \geq 1$, $y \geq 1$) desorbed (Ha = Cl, Br), simulated for (a) Si/Cl and (b) Si/Br systems with different ion energies of E_i = 20–500 eV and neutral-to-ion flux ratios of Γ_n^0/Γ_i^0 = 0–100. Note that "Si_xHa_y" in the legend indicates Si_xHa_y species ($x \geq 2$, $y \geq 1$). The yield or stoichiometry concerned includes the contribution of incident Ha^+ ion reflected from the surface on incidence, as well as that of adsorbates and surface reaction products desorbed through ion incidence: $Y_{Ha} = R_{Ha^+} + Y_{ha} + Y_{ha/Si}$, where $Y_{ha} = \sum_{x=1,2} xY(Ha_x)$ and $Y_{ha/Si} = \sum_{x\geq1, y\geq1} yY(Si_xHa_y)$. Note that the Si yield as in Figs. 3–5 is given by $Y_{Si} = \sum_{x\geq1, y\geq0} xY(Si_xHa_y)$.

number of incoming Ha atoms is >1 (a Ha^+ ion and a set of Ha neutrals) during one cycle of the present MD calculation, where a part of incident neutrals stick on surfaces, while the remaining is reflected or reemitted from surfaces on incidence. For $\Gamma_n^0/\Gamma_i^0 \geq 1$, the Ha yield Y_{Ha} increases with increasing E_i and Γ_n^0/Γ_i^0, corresponding to the increase of the Si yield Y_{Si} and thus the increased desorption of products Si_xHa_y (as in Fig. 4).

It is further noted that for any Γ_n^0/Γ_i^0 in Si/Cl system, the Cl yield Y_{Cl} at low $E_i = 20$ eV consists primarily of the contribution of incident Cl^+ ion reflected from the surface on incidence; and at increased E_i, the reflection is reduced, the desorption of adsorbates Cl_x is increased, and the desorption of surface reaction products Si_xCl_y is further increased. A comparison between Si/Cl and Si/Br systems indicates that for any E_i and Γ_n^0/Γ_i^0, the contribution of reflected Ha^+ ion to the yield Y_{Ha} is relatively small in Si/Br, as compared to that in Si/Cl, owing to relatively small reflection probabilities R_{Ha^+} for heavier Br^+; moreover, for $\Gamma_n^0/\Gamma_i^0 \geq 1$, the Ha yield Y_{Ha} is smaller in Si/Br, similarly to the Si yield Y_{Si} as in Fig. 4. In Si/Br system, the Br yield is $Y_{Br} < 1$ at $E_i = 20$ eV for $\Gamma_n^0/\Gamma_i^0 = 1$ and 10 and at $E_i = 50$ eV for $\Gamma_n^0/\Gamma_i^0 = 1$; this also suggests some deficiency that may still remain in the improved SW potential for Si/Br[35,37] at low E_i (<several tens of eV), as mentioned in the preceding text for the Si yield Y_{Si} with respect to Figs. 4 and 5.

Figure 7 shows the ion-induced halogen desorption yield ($Y_{ha} + Y_{ha/Si}$) per ion impact as a function of the square root of the ion incident energy, $\sqrt{E_i}$, simulated for Si/Ha (Ha = Cl, Br) systems with different ion energies of $E_i = 10$–500 eV and neutral-to-ion flux ratios of $\Gamma_n^0/\Gamma_i^0 = 0$–100. The results indicate that in both systems, the ion-induced Ha yield exhibits similar behavior to that of the ion-induced Si yield Y_{Si} as in Fig. 5; in practice, the yield ($Y_{ha} + Y_{ha/Si}$) increases almost linearly with $\sqrt{E_i}$, where a transition point occurs at around $E_i \approx 100-300$ eV (increased for increased Γ_n^0/Γ_i^0) in Si/Cl. Also shown in the figure are the ion-induced desorption yields $Y_{ha} = \sum_{x=1,2} xY(Ha_x)$ for adsorbates Ha_x, which are appreciated to be important for the site balance of halogen adsorbed on surfaces being etched at low $E_i < 50$ eV, in plasma-surface interactions and the feature profile evolution during plasma etching.[72,73] Although the known data on ($Y_{ha} + Y_{ha/Si}$) and Y_{ha} are remarkably limited, the present MD results agree approximately with the data previously estimated in plasma etching experiments of Si in Cl_2 at $E_i \approx 50$ eV:[74,75] ($Y_{ha} + Y_{ha/Si}$) ≈ 3 with $Y_{Si} \approx 0.4$, which gives $Y_{ha} \approx 1.4$ assuming that the etch products desorbed are $SiCl_4$.

D. Surface coverage, stoichiometry, and depth profile

Figure 8 shows the surface coverage of Ha atoms adsorbed and $SiHa_x$ layer thickness (FWHM) as a function of the square root of the ion incident energy, $\sqrt{E_i}$, simulated for Si/Ha (Ha = Cl, Br) systems with different ion energies of $E_i = 10-500$ eV and neutral-to-ion flux ratios of $\Gamma_n^0/$

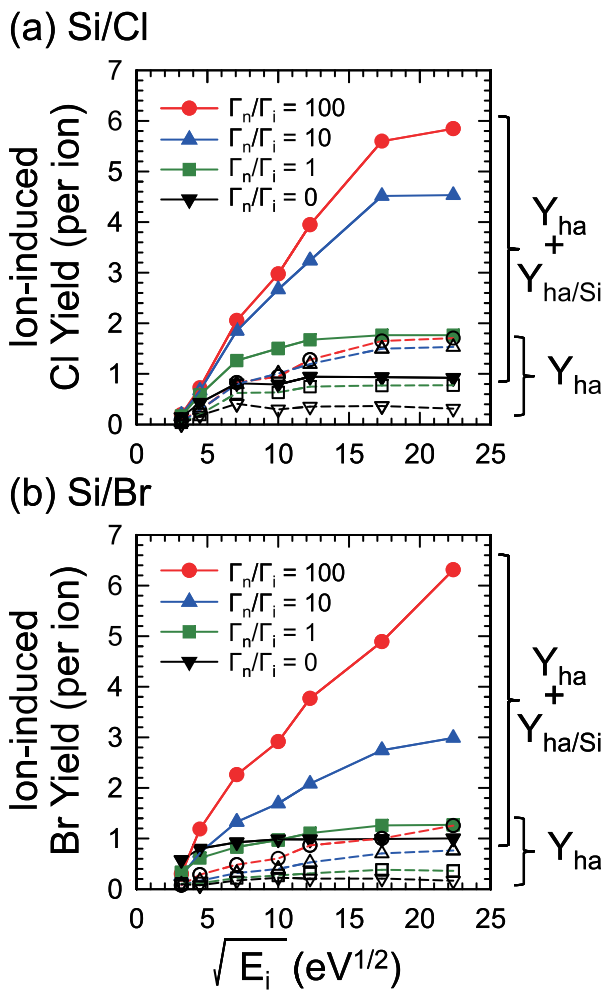

FIG. 7. Ion-induced halogen desorption yield ($Y_{ha} + Y_{ha/Si}$) per ion impact as a function of the square root of the ion incident energy, $\sqrt{E_i}$, simulated for (a) Si/Cl and (b) Si/Br systems with different ion energies of $E_i = 10-500$ eV and neutral-to-ion flux ratios of $\Gamma_n^0/\Gamma_i^0 = 0-100$. Also shown are the ion-induced desorption yields $Y_{ha} = \sum_{x=1,2} xY(Ha_x)$ for adsorbates Ha_x.

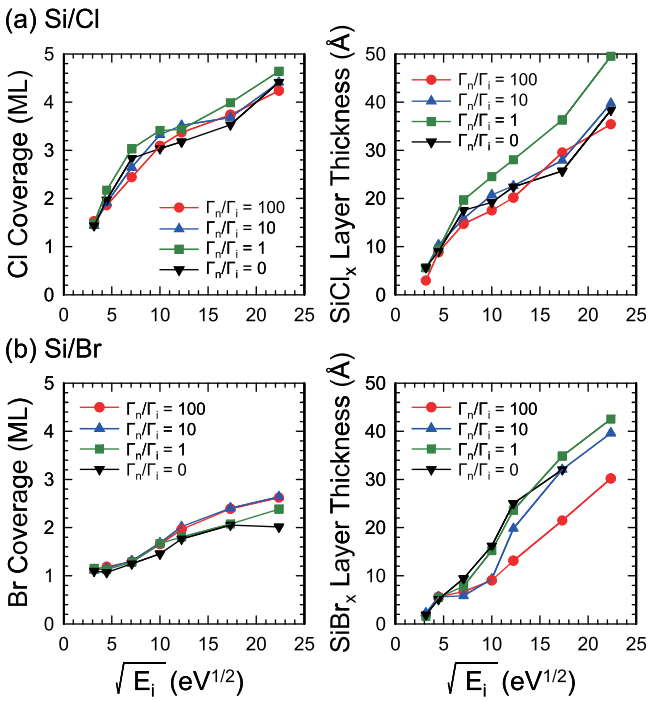

FIG. 8. Surface coverage of Ha atoms adsorbed and $SiHa_x$ layer thickness (FWHM) (Ha = Cl, Br) as a function of the square root of the ion incident energy, $\sqrt{E_i}$, simulated for (a) Si/Cl and (b) Si/Br systems with different ion energies of $E_i = 10-500$ eV and neutral-to-ion flux ratios of $\Gamma_n^0/\Gamma_i^0 = 0-100$. Note that 1 ML for coverage corresponds to the areal density of 6.78×10^{14} atoms/cm^2.

$\Gamma_i^0 = 0-100$. Here 1 ML for coverage corresponds to the areal density of 6.78×10^{14} atoms/cm^2. The results indicate that in both systems, the Ha coverage increases with increasing E_i, while it remains almost unchanged for varying Γ_n^0/Γ_i^0 at a given E_i (as partly seen in Fig. 3); on the other hand, the $SiHa_x$ layer thickness increases with increasing E_i, while it tends to be slightly decreased for increased Γ_n^0/Γ_i^0 at a given E_i (as partly seen in Figs. 2 and 3). In effect, the thickness of halogenated surface $SiHa_x$ layers is generally expected to be determined primarily by the Ha^+ incident energy E_i because the penetration depth of incident Ha^+ ions into substrates is determined by E_i, increasing with increasing E_i; and the neutral-to-ion flux ratio Γ_n^0/Γ_i^0 is assumed to have an incidental effect on the $SiHa_x$ layer thickness because the desorption of surface reaction products Si_xHa_y therefrom is enhanced for increased Γ_n^0/Γ_i^0 as a result of enhanced etching reactions. Moreover, the surface coverage of Ha is also expected to be determined primarily by E_i because the amount of Ha atoms contained in surface $SiHa_x$ layers is determined by the following: the surface reflection probability of incident Ha^+ ions, the amount of incident Ha neutrals that stick on surfaces without reflection/reemission therefrom (per ion impact, or per one cycle of the MD calculation), and the ion-induced desorption yield for Ha atoms adsorbed ($Y_{ha} + Y_{ha/Si}$ as in Fig. 7); in practice, the first one would depend primarily on E_i, the second one on coverage and Γ_n^0/Γ_i^0, and the last one on E_i and coverage.

A comparison between Si/Cl and Si/Br systems indicates that for any E_i and Γ_n^0/Γ_i^0, the Ha coverage and $SiHa_x$ layer thickness are both smaller in Si/Br (as partly seen in Figs. 2 and 3), which is attributed to the shallower penetration depth of Br into substrates, arising from its larger atomic radius. The mean (volume averaged) concentration of Ha atoms in surface $SiHa_x$ layers simulated remains almost unchanged for varying E_i, while it increases slightly with increasing Γ_n^0/Γ_i^0; e.g., at $E_i = 100$ eV for $\Gamma_n^0/\Gamma_i^0 = 0$ and 100, the respective Ha concentrations are estimated to be ~1.0 and 1.2×10^{22} cm^{-3} in Si/Cl and ~0.6 and 1.2×10^{22} cm^{-3} in Si/Br (the density of crystalline Si is $n_{Si} \approx 5.0 \times 10^{22}$ cm^{-3}). Thus it follows that in a sense, the increase in Ha coverage is primarily a reflection of the increase in $SiHa_x$ layer thickness; in effect, the former increases with increasing E_i almost independently of Γ_n^0/Γ_i^0, while the latter increases with increasing E_i and decreases slightly with increasing Γ_n^0/Γ_i^0. It is further noted that in Si/Cl system, the Cl coverage presently simulated, e.g., ~2.5 and 3.7×10^{15} cm^{-2} at $E_i = 50$ and 300 eV (for $\Gamma_n^0/\Gamma_i^0 = 100$), respectively, is in excellent agreement with the previous laser-induced thermal desorption[11] and x-ray photoelectron spectroscopy (XPS)[12] analyses of Si surfaces etched in Cl_2 plasmas (typically ~1.8 and 3.5×10^{15} cm^{-2} at $E_i \approx 40$ and 280 eV, respectively, in XPS). Moreover, the $SiCl_x$ layer thickness simulated, e.g., ~15 and 30 Å at $E_i = 50$ and 300 eV (for $\Gamma_n^0/\Gamma_i^0 = 100$), respectively, is also in excellent agreement with the XPS[12,14] and spectroscopic ellipsometry[13] analyses of Si surfaces etched in Cl_2 plasmas (typically ~13 and 25 Å at $E_i \approx 40$ and 280 eV, respectively, in XPS).

Figure 9 shows the total numbers of Si–Ha_x bonds ($x \geq 1$) contained per unit area in surface $SiHa_x$ layers, together with the stoichiometry of them, simulated for Si/Ha (Ha = Cl, Br) systems with different ion energies of $E_i = 20$–500 eV and

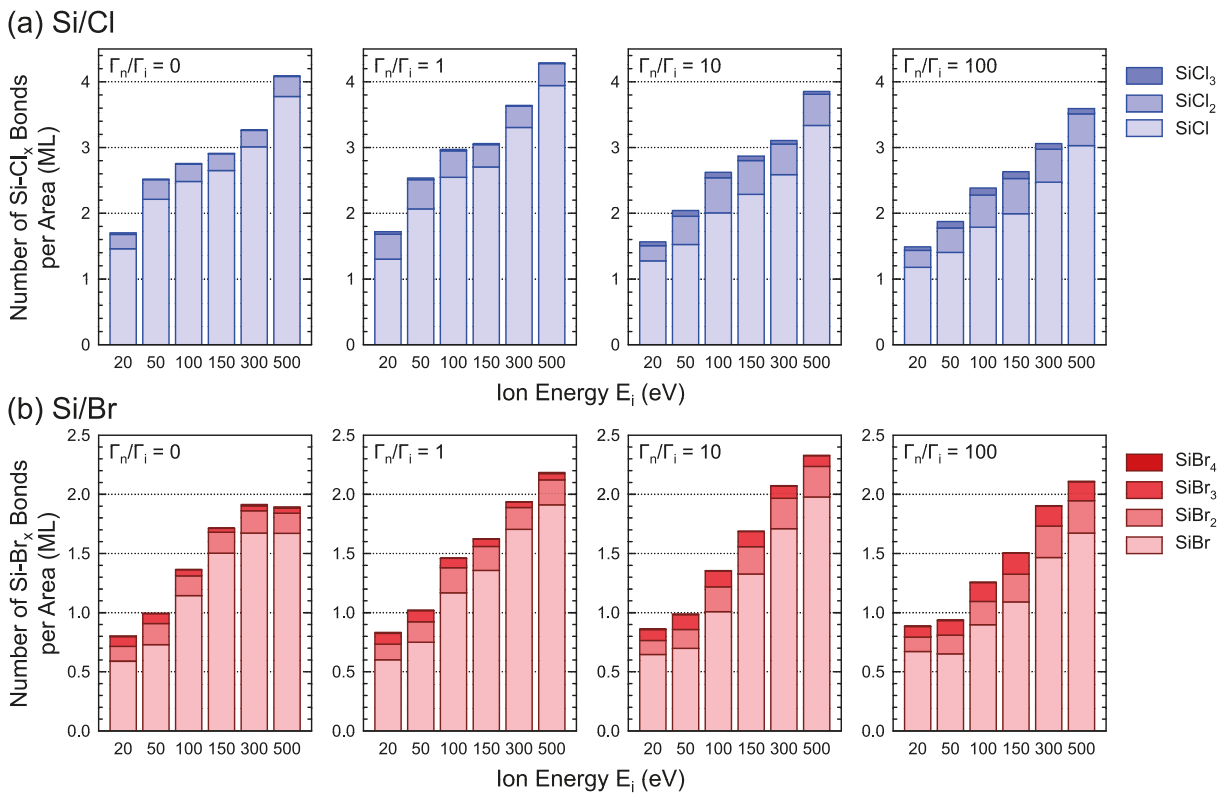

FIG. 9. Total numbers of Si−Ha_x bonds ($x \geq 1$) contained per unit area in surface $SiHa_x$ layers (Ha = Cl, Br), together with the stoichiometry of them, simulated for (a) Si/Cl and (b) Si/Br systems with different ion energies of $E_i = 20-500$ eV and neutral-to-ion flux ratios of $\Gamma_n^0/\Gamma_i^0 = 0-100$. Note that 1 ML corresponds to the areal density of 6.78×10^{14} bonds/cm^2.

neutral-to-ion flux ratios of $\Gamma_n^0/\Gamma_i^0 = 0$–100. Here 1 ML corresponds to the areal density of 6.78×10^{14} bonds/cm^2. The Si−Ha$_x$ bonds are assumed to be counted when there are x Ha atoms within a sphere of $1.2r_0$ radius surrounding the Si atom concerned, where r_0 is the equilibrium distance of the two-body potential function for Si−Ha (as given earlier with respect to Fig. 2); the number of Si−Ha$_x$ bonds or SiHa$_x$ species in surface SiHa$_x$ layers thus counted is a little smaller than that of Ha atoms therein as in the preceding Fig. 8. The results indicate that for any E_i and Γ_n^0/Γ_i^0 in both systems, the predominant surface product species is SiHa, followed by SiHa$_2$ and then SiHa$_3$, where the number of higher halogenated species SiHa$_3$ is very small, and that of fully halogenated SiHa$_4$ is further extremely small (SiCl$_4$ was not observed, and SiBr$_4$ accounted for <0.2% of the total) in the present simulations. The percentage of surface products SiHa$_x$ containing fewer Ha atoms increases with increasing E_i, while that of SiHa$_x$ containing more Ha atoms is increased for increased Γ_n^0/Γ_i^0 at a given E_i, similarly to the stoichiometry of product species Si$_x$Ha$_y$ ($x \geq 1$, $y \geq 1$) desorbed as in Figs. 4 and 6; in effect, higher halogenated species SiHa$_2$ and SiHa$_3$ in surface SiHa$_x$ layers are expected to be more abundant for higher Γ_n^0/Γ_i^0, where the increased supply of neutral reactants onto surfaces would further increase the surface halogenation/chlorination.

However, the stoichiometry of surface SiHa$_x$ layers is seen to not correlate directly with that of product species Si$_x$Ha$_y$ desorbed from surfaces; in effect, the surface stoichiometry remains relatively unchanged for varying E_i and Γ_n^0/Γ_i^0, and the percentage of low halogenated SiHa is relatively large in SiHa$_x$ layers for any E_i and Γ_n^0/Γ_i^0, as compared to the product stoichiometry. This may be attributable to the so-called chemically enhanced physical sputtering in the presence of ion-induced chemical reactions:[43] the surface SiHa$_x$ layers are formed primarily by chemical reactions of Ha atoms adsorbed, while the desorption of surface reaction products Si$_x$Ha$_y$ is enhanced by the sputtering through ion incidence, where larger molecules including higher-halogenated product species would be formed at or near the surface.

A comparison between Si/Cl and Si/Br systems indicates that for any E_i and Γ_n^0/Γ_i^0, the total number of Si−Ha$_x$ bonds ($x \geq 1$) contained in surface SiH$_x$ layers is smaller in Si/Br, owing to the less chemical reactivity of Br on Si. Moreover, high-halogenated surface product species SiHa$_3$ and SiHa$_4$ are more abundant in Si/Br, similarly to the product stoichiometry as in Figs. 4 and 6; this would correlate with higher concentrations of Ha atoms in the near-surface region of thinner SiHa$_x$ layers in Si/Br (as seen earlier in Fig. 2) and thus with higher percentages of high-halogenated surface products SiHa$_3$ and SiHa$_4$ therein (as clearly seen in the following text in Fig. 10). It is further noted that in Si/Cl system, the number of SiCl$_x$ species in surface SiCl$_x$ layers presently simulated is, e.g., [SiCl]:[SiCl$_2$]:[SiCl$_3$] = 1.0:0.13:0.003 and 1.0:0.08:0.002 at $E_i = 50$ and 300 eV for $\Gamma_n^0/\Gamma_i^0 = 0$, respectively, and [SiCl]:[SiCl$_2$]:[SiCl$_3$] = 1.0:0.26:0.07 and 1.0:0.20:0.035 at $E_i = 50$ and 300 eV for $\Gamma_n^0/\Gamma_i^0 = 100$, respectively. This surface stoichiometry simulated for $\Gamma_n^0/\Gamma_i^0 = 100$ is in excellent agreement with the previous XPS analysis of Si surfaces etched in Cl$_2$ plasmas (typically, [SiCl]:[SiCl$_2$]:[SiCl$_3$] ≈ 1.0:0.34:0.087 and 1.0:0.32:0.13 at $E_i \approx 40$ and 280 eV, respectively).[12,14]

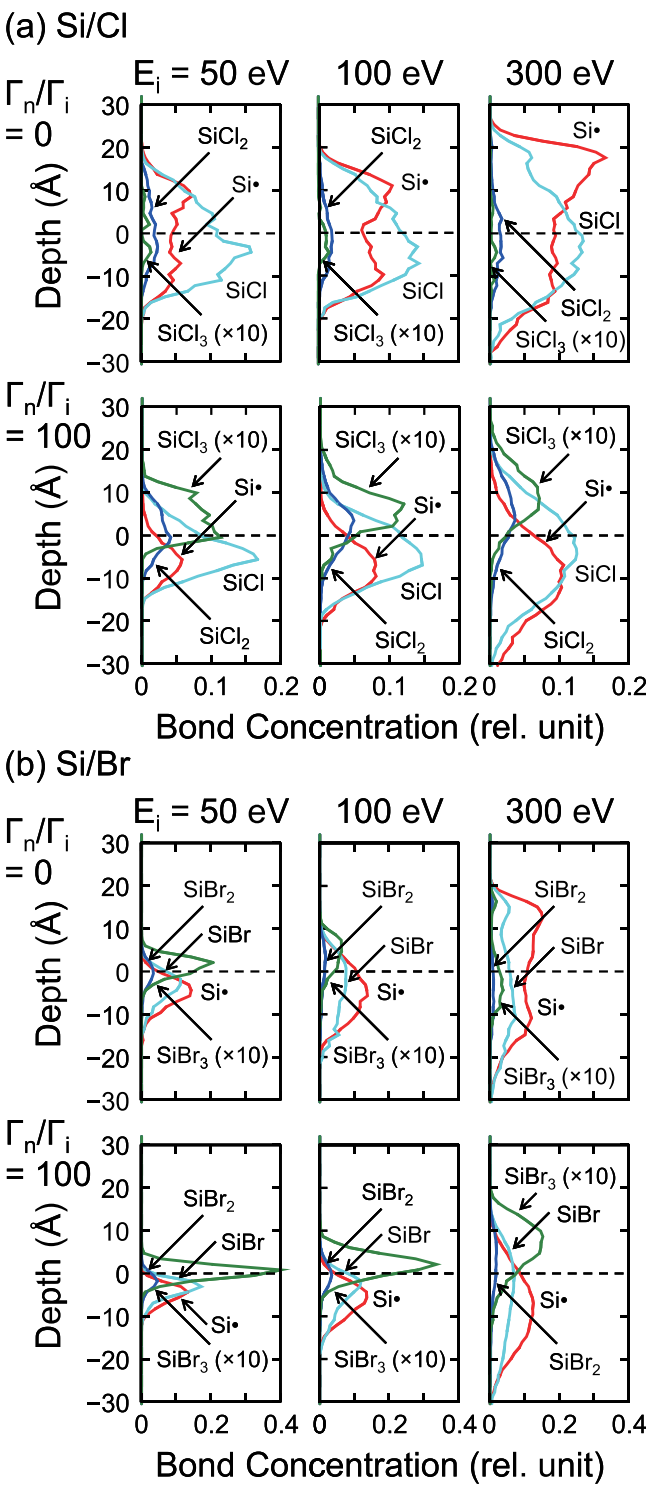

FIG. 10. Depth profiles of Si• and Si−Ha$_x$ bonds ($x \geq 1$) contained in surface SiHa$_x$ layers (Ha = Cl, Br), simulated for (a) Si/Cl and (b) Si/Br systems with different ion energies of $E_i = 50$, 100, and 300 eV and neutral-to-ion flux ratios of $\Gamma_n^0/\Gamma_i^0 = 0$ and 100, corresponding to the side views of the Si(100) surface and the depth profiles of Ha and Si atoms therein as shown in Fig. 2. Here Si• indicates the Si atoms bound to no Ha atoms and having at least one dangling bond, and the figure properties (concentration and depth of zero) are the same as in Fig. 2.

Figure 10 shows the depth profiles of Si• and Si−Ha$_x$ bonds ($x \geq 1$) contained in surface SiHa$_x$ layers, simulated for Si/Ha (Ha = Cl, Br) systems with different ion energies of $E_i = 50$, 100, and 300 eV and neutral-to-ion flux ratios of

$\Gamma_n^0/\Gamma_i^0 = 0$ and 100, corresponding to the side views of the Si(100) surface and the depth profiles of Ha and Si atoms therein as shown earlier in Fig. 2. Here Si• indicates the Si atoms bound to no Ha atoms and having at least one dangling bond, and the figure properties (depth profile and depth of zero) are the same as in Fig. 2. The results indicate that in both systems, the distribution of Si• as well as Si−Ha_x bonds broadens with increasing E_i, while it tends to be narrowed for increased Γ_n^0/Γ_i^0 at a given E_i, corresponding to the tendency of the thickness of surface $SiHa_x$ layers (or the distribution of Ha atoms contained therein) as in Figs. 2, 3, and 8. Moreover, the amount of Si• is seen to increase with increasing E_i, while it is decreased for increased Γ_n^0/Γ_i^0 at a given E_i, similarly to the amount of elemental Si desorbed as in Fig. 4.

It is further noted that for any E_i and Γ_n^0/Γ_i^0 in both systems, the predominant surface product species SiHa is distributed widely in surface $SiHa_x$ layers; on the other hand, higher halogenated species $SiHa_2$ and $SiHa_3$ are distributed in the central region of $SiHa_x$ layers for $\Gamma_n^0/\Gamma_i^0 = 0$, while they tend to be confined to the surface region for $\Gamma_n^0/\Gamma_i^0 = 100$, corresponding to the tendency of the concentration of Ha atoms in $SiHa_x$ layers as in Fig. 2. In effect, the increased supply of neutral reactants onto surfaces would further increase the surface halogenation in the near-surface region. This is also in excellent agreement with the previous XPS analysis of Si surfaces etched in Cl_2 plasmas,[12,14] where higher chlorides $SiCl_2$ and $SiCl_3$ were observed to be confined to the surface region with the predominant chloride SiCl below the surface. A comparison between Si/Cl and Si/Br systems indicates that for any E_i and Γ_n^0/Γ_i^0, the distributions of Si• and Si−Ha_x bonds are narrower in Si/Br, corresponding to thinner $SiBr_x$ layers as seen in Figs. 2, 3, and 8; in addition, higher halogenated/brominated species $SiBr_2$ and $SiBr_3$ tend to be confined to the surface region even for $\Gamma_n^0/\Gamma_i^0 = 0$ at lower $E_i = 50$ and 100 eV, corresponding to the tendency of the concentration of Br atoms in $SiBr_x$ layers.

E. Energy and angular distribution of products and adsorbates desorbed

Products and adsorbates desorbed from surfaces through ion incidence during plasma etching are assumed to have distinct energy and angular distributions. In particular, the energy and angular distribution characteristics of desorbed products are important because they often reach another surfaces in the microstructural feature concerned and then stick or redeposit thereon, which affects the evolution of feature profiles during etching.[72,73] However, only a few studies have so far been concerned with the energy and angular distribution of products and adsorbates desorbed during etching: beam experiments of Ar^+ ion incidence on Si in Cl_2 (showing the energy distribution only)[59,60,62] and MD simulations of Ar^+ incidence on SiO_2[76] and CF_x^+ incidence on SiO_2[77,78] and SiOCH[79] surfaces.

We consider the desorption of products and adsorbates from an infinitesimal surface area at the origin, along with the coordinate system and angles as shown in Fig. 11, where

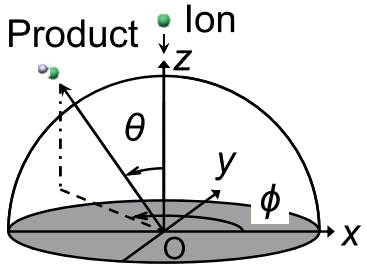

FIG. 11. Coordinate system and angles for the analysis of the energy and angular distribution of products and adsorbates desorbed from surfaces being etched. The ion incidence is taken to be in the vertical ($-z$) direction, where the system is azimuthally symmetric.

the infinitesimal surface of interest corresponds to that of 32.58×32.58 Å^2 in the present MD (Fig. 1). The polar angle θ is the angle of the desorbed velocity with respect to the surface normal, where the ion incidence is taken to be in the vertical ($-z$) direction, and the azimuthal angle ϕ is the angle of it with respect to the vertical (x, z) plane, where the system is azimuthally symmetric. If we assume that atoms and molecules of interest are in thermal equilibrium with surfaces of temperature T_0, their velocity (or speed) and angular distribution leaving the surface is known to be given by a Maxwellian (or Maxwell–Boltzmann) stream[80]

$$F_0(c,\theta)d\Omega\,dc = \frac{2}{\pi}\left(\frac{m}{2k_BT_0}\right)^2 c^3 \exp\left(-\frac{m}{2k_BT_0}c^2\right)\cos\theta\,d\Omega\,dc, \tag{1}$$

where $c = (\sum_{i=x,y,z} c_i^2)^{1/2}$ is the speed of atoms/molecules desorbed, m is the mass of them, $d\Omega = 2\pi\sin\theta\,d\theta$ is the solid angle element concerned, k_B is the Boltzmann constant, and the distribution is normalized such that $\int_0^\infty \int_0^{2\pi} F_0(c,\theta)\,d\Omega\,dc = 1$. Then the distribution is written in the form

$$F_0(c,\theta)d\Omega\,dc = f_0(E)\,g_0(\theta)\,d\Omega\,dE, \tag{2}$$

$$f_0(E) = \frac{1}{(k_BT_0)^2}E\exp\left(-\frac{E}{k_BT_0}\right), \tag{3}$$

$$g_0(\theta) = \frac{\cos\theta}{\pi}, \tag{4}$$

where $E = (1/2)\,m\,c^2$ is the translational energy of atoms/molecules desorbed, and the energy and angular distributions are normalized such that $\int_0^\infty f_0(E)\,dE = 1$ and $\int_0^{2\pi} g_0(\theta)\,d\Omega = \int_0^{\pi/2} g_0(\theta)\,2\pi\sin\theta\,d\theta = 1$, respectively. Note that the range of the translational energy concerned is $0 < E < E_i$, practically.

1. Energy distribution

Figure 12 shows the energy distributions $f(E)/E$ of products $SiHa_x$ ($x = 1-3$) and halogen adsorbate Ha desorbed from surfaces being etched, in the range $0 < E < 10$ eV, obtained from simulations for Si/Ha (Ha = Cl, Br) systems with different ion energies of $E_i = 50$, 150, and 300 eV and neutral-to-ion flux ratios of $\Gamma_n^0/\Gamma_i^0 = 0$ and 100. Here the

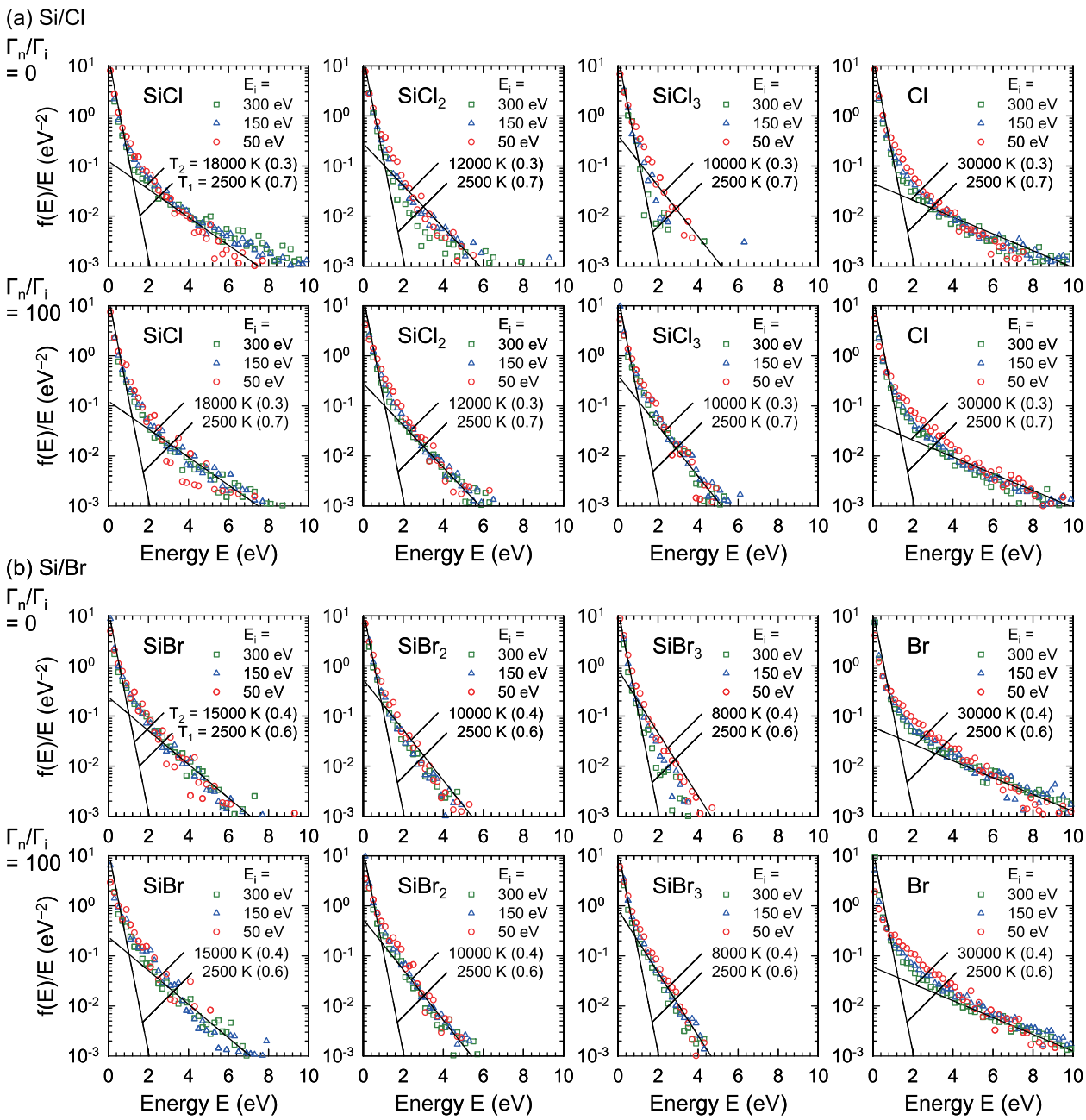

FIG. 12. Energy distributions $f(E)/E$ of products SiH_x ($x = 1-3$) and halogen adsorbate Ha desorbed from surfaces being etched (Ha = Cl, Br), in the range $0 < E < 10$ eV, obtained from simulations for (a) Si/Cl and (b) Si/Br systems with different ion energies of $E_i = 50$, 150, and 300 eV and neutral-to-ion flux ratios of $\Gamma_n^0/\Gamma_i^0 = 0$ and 100. Here the distributions are normalized such that $\int_0^\infty f(E)\,dE = 1$, where the range of the translational energy concerned is practically $0 < E < E_i$, and the data for Ha shown are those for atoms desorbed through ion incidence (not including the contribution of incident Ha^+ ions reflected). Also shown are the two reference curves $C_\alpha f_0^\alpha(E)/E = C_\alpha (k_B T_\alpha)^{-2} \exp(-E/k_B T_\alpha)$ ($\alpha = 1$, 2) of temperature $T_1 \approx 2500$ K and $T_2 \approx 8000$–30 000 K [Eq. (3)]. Note that the two reference distributions $f_0^\alpha(E)$ are taken to be normalized such that $\int_0^\infty [C_1 f_0^1(E) + C_2 f_0^2(E)]\,dE = 1$, where C_1 and C_2 are constants corresponding to the respective fractions of the distribution, being given as numerals in parentheses in the figure [$C_1 + C_2 = 1$, $\int_0^\infty f_0^\alpha(E)\,dE = 1$].

distributions are normalized such that $\int_0^\infty f(E)\,dE = 1$, and each data point for a given E reflects the number (per unit energy) of atoms/molecules of interest desorbed per ion impact with translational energies between $E - (\Delta E)/2$ and $E + (\Delta E)/2$, counted with $\Delta E = 0.2$ eV for more than 15 000 impacts; in addition, the data for Ha shown are those for atoms desorbed through ion incidence (not including the contribution of incident Ha^+ ions reflected). Also shown in the figure are the two reference curves $C_\alpha f_0^\alpha(E)/E = C_\alpha (k_B T_\alpha)^{-2} \exp(-E/k_B T_\alpha)$ ($\alpha = 1$, 2) of temperature $T_1 \approx 2500$ K and $T_2 \approx 8000-30\,000$ K [Eq. (3)]; note that the two reference distributions $f_0^\alpha(E)$ are taken to be normalized such that $\int_0^\infty [C_1 f_0^1(E) + C_2 f_0^2(E)]\,dE = 1$, where C_1 and C_2 are constants corresponding to the respective fractions of the distribution, being given as numerals in parentheses in the figure [$C_1 + C_2 = 1$, $\int_0^\infty f_0^\alpha(E)\,dE = 1$].

The results indicate that in both systems, the energy distributions may be approximated by two Maxwellians of low T_1 and high T_2: $f(E) \approx C_1 f_0^1(E) + C_2 f_0^2(E)$, where the first Maxwellian stream $f_0^1(E)$ with $T_1 \approx 2500$ K is seen to occur with a fraction $C_1 \approx 0.6-0.7$, irrespective of species as well as of E_i and Γ_n^0/Γ_i^0. On the other hand, the second one $f_0^2(E)$

with high $T_2 \approx 8000-30\,000$ K is seen to occur with a fraction $C_2 \approx 0.3-0.4$, depending significantly on species desorbed; in effect, the temperature T_2 is higher for lighter species (T_2 is the highest for light Ha, followed by those for SiHa, $SiHa_2$, and $SiHa_3$ in decreasing order), while it seems to be not so sensitive to E_i and Γ_n^0/Γ_i^0. A comparison between Si/Cl and Si/Br systems indicates that the fraction C_1 of the distribution $f_0^1(E)$ is slightly smaller [or C_2 of $f_0^2(E)$ is slightly larger] in Si/Br and that the temperature T_2 for $SiHa_x$ appears to be slightly lower in Si/Br, while those for light Ha are nearly the same in both systems. Similar results were also obtained for Si, $SiHa_4$, and Ha_2 as listed in Table I (not shown in Fig. 12): $T_2 \approx 40\,000$ K ($C_2 \approx 0.6$) for light elemental Si is the highest, followed by those for Ha, Ha_2, SiHa, $SiHa_2$, $SiHa_3$, and $SiHa_4$ in decreasing order; and $T_2 \approx 7000$ K ($C_2 \approx 0.4$) for heavy $SiBr_4$ is the lowest in all species concerned. The average energies of the species desorbed are evaluated in the table as $\overline{E_0} = C_1(3/2)\,k_B T_1 + C_2(3/2)\,k_B T_2$ [$\approx C_2(3/2)\,k_B T_2$, practically, because of $C_1 \sim C_2$ and $T_1 \ll T_2$]; note that the respective energies $\overline{E_0}$ tend to be similar in both systems, owing to larger C_2 while lower T_2 in Si/Br, and that the distributions $f(E)$ of $SiCl_4$ were not well obtained in the present MD because of extremely small yields of it as mentioned earlier with respect to Fig. 4.

The temperature $T_1 \approx 2500$ K is surprisingly very similar to those previously evaluated from time-of-flight distributions of sputtered $SiCl_x$ ($x = 1-3$) in beam experiments of 100-eV Ar^+ ion incidence on Si in Cl_2 [$T = 2450$, 2500, and 2100 (or 2700) $\pm$ 150 K for SiCl, $SiCl_2$, and $SiCl_3$ (or $SiCl_4$), respectively];[62] in the experiments, a transition from a collision-cascade to a Maxwell–Boltzmann distribution was shown to occur at $E_i \approx 250$ eV as the Ar^+ ion energy was decreased from $E_i = 500$ to 100 eV, where the Maxwell–Boltzmann distributions of high $T > 2000$ K at low $E_i \approx 100$ eV were attributed to the desorption or evaporation of surface reaction products $SiCl_x$ from an ion-induced local hot spot.[62] Note that the energy distribution of atoms/molecules sputtered by a collision-cascade mechanism is often given by $f_c(E) = CE/(E+U)^3$,[43,62,81] where U is the effective surface binding energy, C is a constant for normalization, and the distribution peaks at $E = U/2$. The beam experiments further showed that for heavier Xe^+ ion bombardment on Si in Cl_2, the transition occurred at higher $E_i \approx 500-2000$ eV than for Ar^+, and the surface temperature of the hot spot (evaluated from the distribution of SiCl) was lower than for Ar^+, increasing from $T = 1250$ to 1800 K as the Xe^+ ion energy was decreased from $E_i = 2000$ to 150 eV.[62] These were explained in terms of the effective surface binding energy U which the species have to overcome to be sputtered or ejected from surfaces:[62] the temperature T, characterizing the Maxwell–Boltzmann distribution of sputtered species, is assumed to be correlated with U, which is expected to be lower for higher chlorinated molecules; moreover, U is also expected to be lowered at increased E_i, because the energy deposition in surface layers increases thereat, where in turn more damage is formed, more excitation of surface-bound species takes place, and then U is lowered; similarly, the energy deposition in surface layers is higher under heavier ion bombardment at the same ion energy,[82–84] thus resulting in lower U under that condition.

A Maxwellian stream with much higher $T \gg 2000$ K has not been reported so far numerically as well as experimentally. However, the present MD results of the temperature T_2 ($\approx 7000-40\,000$ K, depending significantly on species of products and adsorbates desorbed and slightly on incident species) may be consistent with the previous beam experiments of Ar^+ and Xe^+ ion incidences on Si in Cl_2 as concerned in the preceding text,[62] to some extent: the temperature T_2 is higher for lighter species (or lower halogenated species) and is lower for heavier Br^+ incidence. Moreover, the maximum of the energy distribution is often assumed to suggest the effective surface binding energy U of sputtered species;[43] in the present MD, the maximum of the Maxwellian $f_0^1(E)$ occurring at $E = k_B T_1$ suggests $U_1 \approx 0.21$ eV irrespective of species, while that of $f_0^2(E)$ at $E = k_B T_2$ suggests $U_2 \approx 0.6-3.4$ eV depending on incident as well as desorbed species (as also listed in Table I). These U_2 values appear to be in agreement with the previous beam experiments of Ar^+ ion incidence on Si in Cl_2,[59,60,62] which gave $U \approx 0.3$ eV for SiCl and $SiCl_2$ (corresponding to weakly bound molecules), while $U \approx$ a few eV for Si and Cl (expected for sputtering of strongly bound atoms).

TABLE I. Characteristic temperatures T_α and coefficients C_α for the two reference distributions $f_0^\alpha(E)$ ($\alpha = 1, 2$) approximating the energy distributions $f(E)$ of products $SiHa_x$ ($x = 0$–4) and halogen adsorbates Ha_x ($x = 1, 2$) desorbed from surfaces being etched, as in Fig. 12: $f(E) \approx C_1 f_0^1(E) + C_2 f_0^2(E)$.

System	Species	m/e (amu)	T_1 (K)	C_1	T_2 (K)	C_2	$\overline{E_0}$ (eV)[a]	U_2 (eV)[b]
Si/Cl	Si	28	2500	0.4	40 000	0.6	3.2	3.4
	SiCl	63	2500	0.7	18 000	0.3	0.92	1.5
	$SiCl_2$	98	2500	0.7	12 000	0.3	0.69	1.0
	$SiCl_3$	133	2500	0.7	10 000	0.3	0.61	0.86
	$SiCl_4$[c]	168	…	…	…	…	…	…
	Cl	35	2500	0.7	30 000	0.3	1.4	2.5
	Cl_2	70	2500	0.7	18 000	0.3	0.92	1.5
Si/Br	Si	28	2500	0.4	40 000	0.6	3.2	3.4
	SiBr	108	2500	0.6	15 000	0.4	0.97	1.2
	$SiBr_2$	188	2500	0.6	10 000	0.4	0.71	0.86
	$SiBr_3$	268	2500	0.6	8000	0.4	0.61	0.68
	$SiBr_4$	348	2500	0.6	7000	0.4	0.56	0.60
	Br	80	2500	0.6	30 000	0.4	1.7	2.5
	Br_2	160	2500	0.6	18 000	0.4	1.1	1.5

[a]Average energy evaluated as $\overline{E_0} = C_1(3/2)\,k_B T_1 + C_2(3/2)\,k_B T_2$.
[b]Effective surface binding energy evaluated as $U_2 = k_B T_2$; the other one $U_1 = k_B T_1 \approx 0.21$ eV irrespective of species.
[c]Distributions $f(E)$ of $SiCl_4$ were not well obtained, because of extremely small yields of it in the present MD.

2. Mean energy

Figure 13 shows the mean energies $\bar{E}$ of products $SiHa_x$ ($x = 0-4$) and halogen adsorbates Ha_x ($x = 1, 2$) desorbed from surfaces being etched, obtained from simulations for Si/Ha (Ha = Cl, Br) systems with different ion energies of $E_i = 50$, 150, and 300 eV and neutral-to-ion flux ratios of $\Gamma_n^0/\Gamma_i^0 = 0$ and 100. Here $\bar{E}$ is the arithmetic average of the translational energy E of atoms/molecules of interest

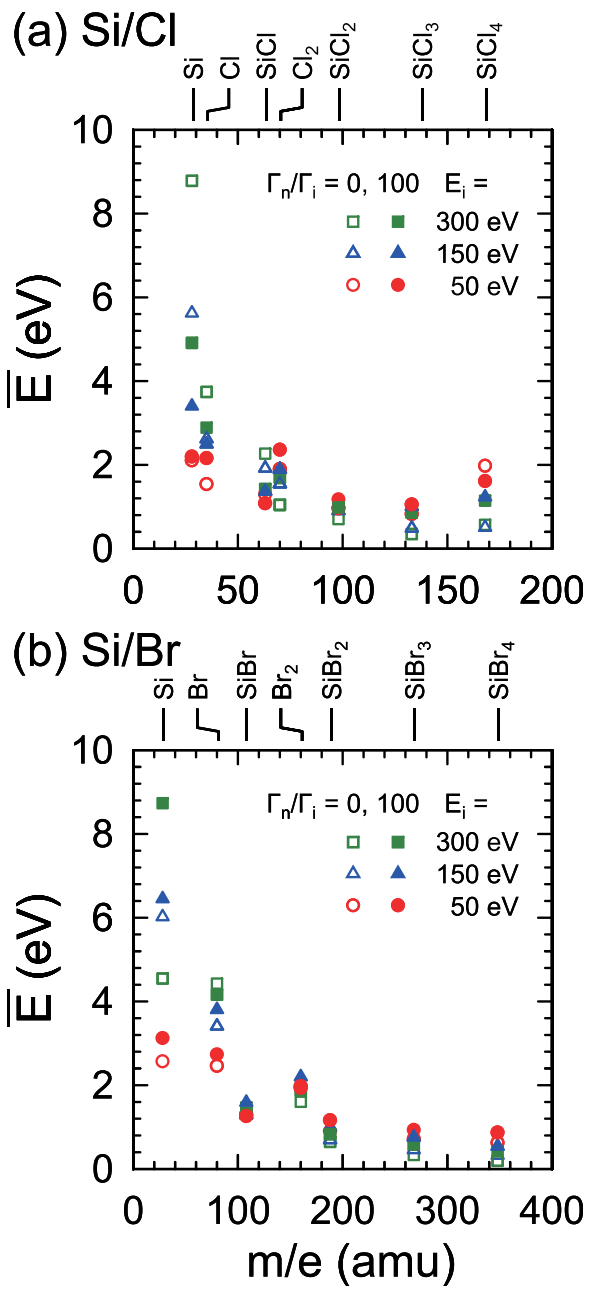

FIG. 13. Mean energies $\bar{E}$ of products $SiHa_x$ ($x = 0$–4) and halogen adsorbates Ha_x ($x = 1$, 2) desorbed from surfaces being etched (Ha = Cl, Br), obtained from simulations for (a) Si/Cl and (b) Si/Br systems with different ion energies of $E_i = 50$, 150, and 300 eV and neutral-to-ion flux ratios of $\Gamma_n^0/\Gamma_i^0 = 0$ and 100. Note that the $\bar{E}$ values of $SiCl_4$ might not be well obtained statistically, owing to extremely small yields of it in the present MD.

desorbed through ion impact (counted for more than 15 000 impacts), and the $\bar{E}$ values of $SiCl_4$ might not be well obtained statistically owing to the same reason as its distributions $f(E)$. The results indicate similar tendencies to those of the temperature T_2 as mentioned in the preceding text (apart from $SiCl_4$): in both systems, the mean energy $\bar{E}$ is higher for lighter species of $SiHa_x$ and Ha_x, although the respective energies $\bar{E}$ tend to be similar in both (similarly to the average energy $\overline{E_0}$ as in Table I). It is further noted that in both systems, the dependence of $\bar{E}$ on E_i is seen to be relatively significant as compared to that of T_2 as in the preceding Fig. 12: $\bar{E}$ is higher at higher E_i for light elemental Si and Ha and slightly higher at higher E_i for SiHa, while it appears to be slightly higher at lower E_i for Ha_2 and $SiHa_x$ ($x \geq 2$); however, $\bar{E}$ seems to be still not so sensitive systematically to Γ_n^0/Γ_i^0.

The mean energy $\bar{E}$ is expected to be approximately equal to the average energy $\overline{E_0}$, in the situation where the energy distribution $f(E)$ is approximated totally by two Maxwellians, $f(E) \approx C_1 f_0^1(E) + C_2 f_0^2(E)$ in the range $0 < E < E_i$; in effect, $\bar{E} \approx \overline{E_0}$ for all $SiHa_x$ and Ha_x species of interest in both Si/Cl and Si/Br systems, apart from a marked deviation $\bar{E} > \overline{E_0}$ that is seen in Fig. 13 for light elemental Si and Ha under high-energy ($E_i > 150$ eV) ion incidence. The deviation concerned is larger for Si than for Ha and is larger at higher E_i, which was found to arise from high-energy tails (at $E > 10$ eV) of the distribution $f(E)$ deviating from the second Maxwellian $C_2 f_0^2(E)$, thus reflecting the contribution of sputtering of strongly bound Si and Ha atoms (as inferred from the temperature T_2 or binding energy U_2 in Sec. III E 1). In practice, the high-energy tails were more significant for Si than for Ha and more significant at increased E_i, which required an additional collision-cascade distribution $f_c(E)$ contributing for <10% to the total fit [note that $f_c(E)$ falls off as E^{-2} at $E \gg U$, which is relatively gradual as compared to the Maxwellian $f_0(E)$ that falls off as $E\exp(-E)$ at $E \gg k_B T_0$].

3. Angular distribution

Figure 14 shows the angular distributions $g(\theta)$ of product $SiHa_2$ and halogen adsorbate Ha desorbed from surfaces being etched, in the range $0 < \theta < \pi/2$, obtained from simulations for Si/Ha (Ha = Cl, Br) systems with different ion energies of $E_i = 50$, 100, and 300 eV and neutral-to-ion flux ratios of $\Gamma_n^0/\Gamma_i^0 = 0$ and 100. Here the distributions are normalized such that $\int_0^{\pi/2} g(\theta)\, 2\pi \sin\theta\, d\theta = 1$, and each data point for a given θ reflects the number (per unit solid angle) of atoms/molecules of interest desorbed per ion impact with polar angles between $\theta - (\Delta\theta)/2$ and $\theta + (\Delta\theta)/2$, counted with $\Delta\theta = 5°$ for more than 15 000 impacts; in addition, the data for Ha shown are also those for atoms desorbed through ion incidence (not including the contribution of incident Ha^+ ions reflected). Also shown in the figure is the reference curve $g_0(\theta) = (\cos\theta)/\pi$ that is known as the cosine law [Eq. (4)].[80,81]

The results appear to indicate the following tendencies, although statistics of the distribution might be poor at small angles θ in the present MD, owing to small solid angles $d\Omega = 2\pi \sin\theta\, d\theta$ and thus few atoms/molecules desorbed thereat: in both systems, the angular distributions of $SiHa_2$ and Ha are under-cosine at high $E_i = 300$ eV irrespective of Γ_n^0/Γ_i^0, with a tendency to approach cosine and then become over-cosine with decreasing E_i. This tendency is significant for $SiHa_2$, where it is more significant for $\Gamma_n^0/\Gamma_i^0 = 100$ than for $\Gamma_n^0/\Gamma_i^0 = 0$ and is more significant in Si/Br than in Si/Cl. On the other hand, for Ha, the tendency is slightly seen in Si/Cl system (slightly more significant for $\Gamma_n^0/\Gamma_i^0 = 100$ than for $\Gamma_n^0/\Gamma_i^0 = 0$), while it is not seen in Si/Br (the angular distribution of Br remains almost unchanged at under-cosine for varying E_i and Γ_n^0/Γ_i^0). The angular distributions of $SiHa_x$ ($x = 1$, 3, 4) exhibited similar tendencies to that of $SiHa_2$, while those of Si

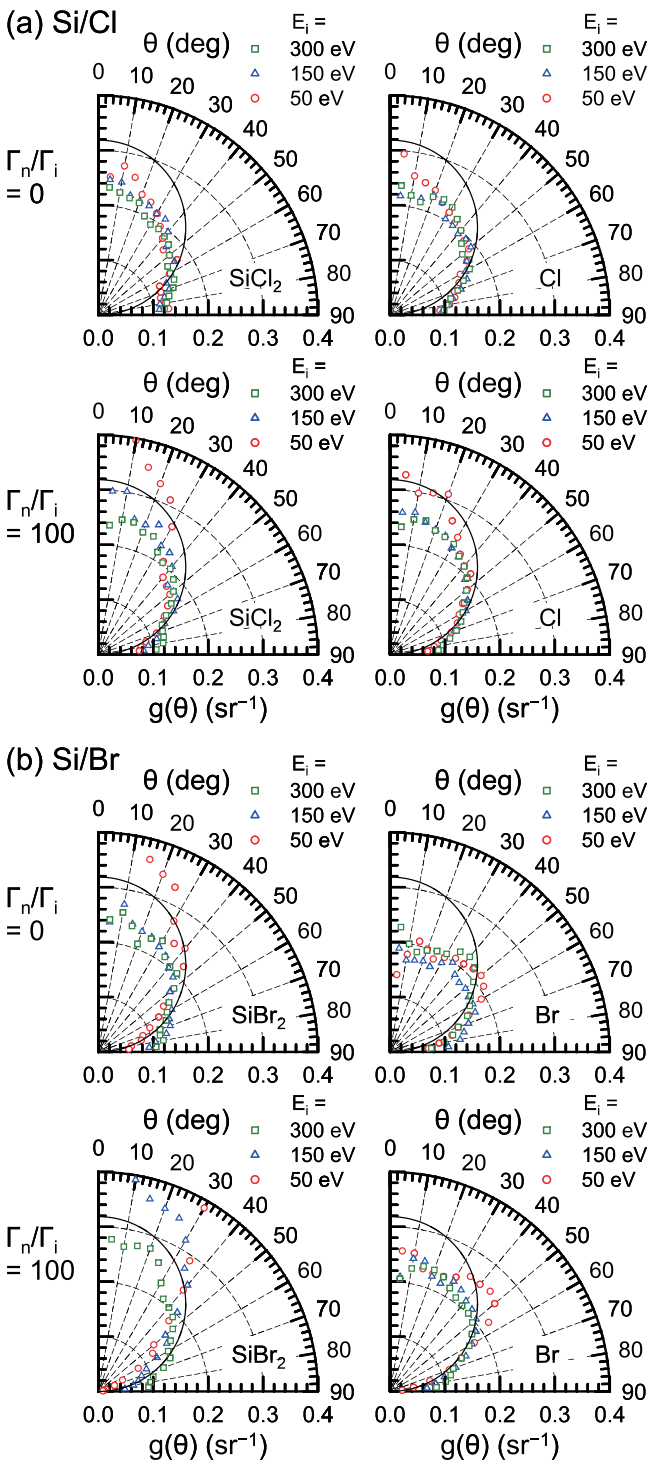

FIG. 14. Angular distributions $g(\theta)$ of product $SiHa_2$ and halogen adsorbate Ha desorbed from surfaces being etched (Ha = Cl, Br), in the range $0 < \theta < \pi/2$, obtained from simulations for (a) Si/Cl and (b) Si/Br systems with different ion energies of $E_i = 50$, 100, and 300 eV and neutral-to-ion flux ratios of $\Gamma_n^0/\Gamma_i^0 = 0$ and 100. Here the distributions are normalized such that $\int_0^{\pi/2} g(\theta)\, 2\pi \sin\theta\, d\theta = 1$, and the data for Ha shown are those for atoms desorbed through ion incidence (not including the contribution of incident Ha^+ ions reflected). Also shown is the reference curve $g_0(\theta) = (\cos\theta)/\pi$ that is known as the cosine law [Eq. (4)].

and Ha_2 exhibited similar tendencies to that of Ha, where the degree of under-cosine was the largest for Si.

The mechanisms for these MD results of the angular distribution are not well understood at present, unfortunately. In effect, the present results are opposite to those generally known for sputtering, for which a number of experimental and theoretical/numerical investigations have shown a distinct under-cosine distribution at low $E_i < 1$ keV, approaching cosine with increasing E_i.[81,85,86] However, a few experiments of sputtering by light H^+ and He^+ ions of 1 and 4 keV showed an over-cosine distribution;[87] moreover, a few theoretical/numerical studies of sub-keV Ar^+ ion sputtering indicated that the distribution consists of an under-cosine contribution produced by ion-in sputtering (sputtering by primary ions directed inside the target) and an over-cosine contribution resulting from ion-out sputtering (sputtering by backscattered ions moving in the outward direction).[88,89] An anisotropic, nonequilibrium distribution like $F(c,\theta) = f_0(E)g(E,\theta)$[88,89] may be required to understand the mechanisms responsible, although there are no experimental and theoretical/numerical data to be compared on the angular distribution of products and adsorbates desorbed during plasma etching.

4. Surface reaction kinetics

The ion bombardment-induced etch processes in plasma etching have been appreciated to consist of physical sputtering and ion-enhanced etching, and the latter has been speculated to consist of the so-called chemically enhanced physical sputtering and chemical sputtering (or, physically enhanced chemical sputtering).[43] In chemically enhanced physical sputtering, the surface reaction layers are assumed to be formed primarily by chemical reactions of reactive neutrals adsorbed in the presence of ion-induced chemical reactions, where the desorption of surface reaction products is enhanced by the sputtering through ion incidence;[43] and the translational energy distribution of atoms/molecules desorbed is often assumed to be a collision-cascade type, where weakly bound molecules are created and desorbed during the same collision cascade.[43] However, if they remain on the surface for a period of time and then desorb during the development of the hot spots, they are expected to have a Maxwell–Boltzmann distribution characterized by a high temperature;[43,62] in these situations, different species desorbed may have Maxwell–Boltzmann distributions with different temperatures depending on the respective surface binding energies.[62] This would correspond to the Maxwellian stream $f_0^2(E)$ with $C_2 \approx 0.3-0.6$ and $T_2 \approx 7000$–$40\,000$ K in the present MD. On the other hand, in chemical sputtering, the surface reaction layers are assumed to be formed primarily by ion-induced chemical reactions in the presence of reactive neutrals, where the desorption of surface reaction products is caused by thermal processes;[43] in these situations, different species are expected to be desorbed or evaporated from the hot spots established on surfaces with Maxwell–Boltzmann distributions characterized by the same temperature.[43,62] This would correspond to the Maxwellian stream $f_0^1(E)$ with $C_1 \approx 0.4-0.7$ and $T_1 \approx 2500$ K in the present MD.

Hence we may conclude that the present MD results of the translational energy distribution reveal the coexistence of the chemically enhanced physical sputtering and chemical sputtering that have so far been speculated to both occur in the ion-enhanced surface reaction kinetics of plasma etching.[43] In the MD simulations, local hot spots should be

formed on surfaces during ion bombardment;[62] at earlier times soon thereafter, the former [concerned with $f_0^2(E)$, T_2] would occur, when atoms/molecules with high kinetic energies that overcome the respective surface binding energies (U_2) desorb from the hot spots during the development of them or during a transient, nonequilibrium state in which the hot spots are rapidly cooling down.[62] Then the latter [concerned with $f_0^1(E)$, T_1] would occur at later times, when atoms/molecules with lower kinetic energies that overcome the surface binding energies lowered (U_1) desorb from the hot spots that have reached a state of equilibrium. The lifetime of the hot spots is assumed to be of the order of 10^{-12} s,[62] being consistent with the system evolving time of 0.7 ps and the following cooling time of 0.3 ps after ion bombardment in the present MD [as mentioned earlier with respect to Fig. 1(b)].

A relevant understanding of the present MD results of the angular distribution will require a further study including experimental measurements of it.

IV. CONCLUSIONS

We have performed classical MD simulations of Cl^+ and Br^+ ions incident on Si(100) surfaces in the presence of incoming Cl and Br neutrals, respectively, using an improved SW potential form, to gain a better understanding of the ion-enhanced surface reaction kinetics during Si etching in Cl- and Br-based plasmas. The ions were taken to be incident normally onto surfaces with translational energies in the range $E_i = 20-500$ eV, where low-energy neutrals of translational energy $E_n = 0.01$ eV were also incident normally thereon with the neutral-to-ion flux ratio in the range $\Gamma_n^0/\Gamma_i^0 = 0-100$; in practice, the MD calculations consisted of a repetition of an ion incidence followed by that of a set of neutrals, to simulate plasma etching environments with simultaneous incidence of energetic ions and neutral reactants. The simulations gave etch fundamentals such as etch yield and threshold, product stoichiometry, desorption yield of halogen adsorbates, energy and angular distributions of products and adsorbates desorbed, and microscopic structures of surface reaction layers (thickness, coverage, stoichiometry, and depth profile).

The MD results indicated that in both Si/Cl and Si/Br systems, the etch or Si yield Y_{Si} increases with increasing E_i, along with the percentage of elemental Si and low-halogenated Si_xHa_y species; and at a given E_i, the yield Y_{Si} is increased for increased Γ_n^0/Γ_i^0, along with the percentage of higher-halogenated Si_xHa_y species, where the threshold E_{th} (estimated from the Y_{Si} versus $\sqrt{E_i}$ curve) is almost independent of Γ_n^0/Γ_i^0. Moreover, the surface coverage of Ha atoms adsorbed increases with increasing E_i, while it remains almost unchanged for varying Γ_n^0/Γ_i^0 at a given E_i; on the other hand, the surface $SiHa_x$ layer thickness increases with increasing E_i, while it tends to be slightly decreased for increased Γ_n^0/Γ_i^0 at a given E_i. The etch yields and thresholds presently simulated were in agreement with the experimental results previously reported for Si etching in Cl_2 and Br_2 plasmas as well as in Cl^+, Cl_2^+, and Br^+ beams, and the product stoichiometry simulated was consistent with that experimentally observed during Ar^+ beam incidence on Si in Cl_2. Moreover, the surface halogen coverage, halogenated surface layer thickness, surface stoichiometry, and depth profile of surface product species simulated for $\Gamma_n^0/\Gamma_i^0 = 100$ were in excellent agreement with the experimental observations depending on E_i reported for Si etching in Cl_2 plasmas; in particular, the simulations fully reproduced the surface stoichiometry including the depth profiles that higher chlorides $SiCl_2$ and $SiCl_3$ tend to be confined to the surface region with the predominant chloride SiCl below the surface.

The MD results also indicated that the yield, coverage, and surface layer thickness are smaller in Si/Br than in Si/Cl system, owing to the larger atomic radius (or smaller penetration depth) and less reactivity of Br on Si; on the other hand, the percentage of higher halogenated species in product and surface stoichiometries is larger in Si/Br, presumably owing to higher concentrations of halogen atoms in the near-surface region of thinner surface layers in Si/Br. These etch fundamentals for Si/Br system would be useful for understanding the Si etching in Br-based plasmas, we believe, because few studies have been concerned with plasma-surface interactions or surface reaction kinetics for Si/Br in experiments as well as simulations.

The MD results further indicated that in both systems, the translational energy distributions ($0 < E < 10$ eV) of products $SiHa_x$ and halogen adsorbates Ha_x desorbed from surfaces being etched are approximated by two Maxwellians of temperature $T_1 \approx 2500$ K and $T_2 \approx 7000-40\,000$ K. The temperature T_2 is significantly higher for lighter species (or lower halogenated species that are expected to have higher surface binding energies), while T_1 is almost independent of species desorbed; in addition, T_2 is slightly lower in Si/Br, and both T_1 and T_2 appear to be not so sensitive to E_i and Γ_n^0/Γ_i^0 over the range investigated. This temperature T_1 was surprisingly very similar to those previously evaluated from time-of-flight distributions of sputtered $SiCl_x$ ($x = 1-3$) in beam experiments of Ar^+ ion incidence on Si in Cl_2. These results of the energy distribution would give evidence of the desorption or evaporation from hot spots formed through the so-called chemically enhanced physical sputtering and chemical sputtering (or physically enhanced chemical sputtering) that have so far been speculated to both occur in the ion-enhanced surface reaction kinetics of plasma etching. In effect, the former is assumed to correspond to the distribution of high T_2, which would occur at earlier times (or during a transient, nonequilibrium state) soon after ion bombardment; on the other hand, the latter is assumed to correspond to the distribution of low T_1, which would occur at later times (or during a state of equilibrium) after the system has reached equilibrium. In addition, the mean energies of desorbed species suggested high-energy tails ($E > 10$ eV) of the distribution deviating from the second Maxwellian of high T_2 for elemental Si and Ha, reflecting the contribution of sputtering of strongly bound atoms; in practice, the high-energy tails were found to be more significant for Si than for Ha and more significant at increased E_i (not so sensitive to Γ_n^0/Γ_i^0), which required an additional collision-cascade distribution contributing for $<10\%$ to the total fit.

The angular distributions of desorbed species were also analyzed to further discuss the surface reaction kinetics concerned; however, the MD results obtained are not well understood at present. A relevant understanding of the mechanisms for the angular distribution will require a further study including experimental measurements of it, because there are no experimental as well as theoretical/numerical data to be compared on the angular distribution of products and adsorbates desorbed during plasma etching.

Further MD studies are now in progress for the effects of ion incidence angle as well as neutral reactant flux on the interaction of Cl^+ and Br^+ ions with Si surfaces.

ACKNOWLEDGMENTS

This work was supported by a Grant-in-Aid for Scientific Research (21110008) on Innovative Areas from the Ministry of Education, Culture, Sports, Science and Technology (MEXT), Japan, and by that (15H03582) from the Japan Society for the Promotion of Science (JSPS). One of the authors (N.N.) was supported by Research Fellowships from the JSPS for Young Scientists. The authors would also like to thank K. Taniguchi (presently at Fujitsu Ltd.) for MD simulations at the beginning stage of this work.

[1]H. Abe, M. Yoneda, and N. Fujiwara, Jpn. J. Appl. Phys. **47**, 1435 (2008).
[2]B. Wu, A. Kumar, and S. Pamarthy, J. Appl. Phys. **108**, 051101 (2010).
[3]V. M. Donnelly and A. Kornblit, J. Vac. Sci. Technol., A **31**, 050825 (2013).
[4]See http://www.itrs.net for International Technology Roadmap for Semiconductors (ITRS) 2013 Update.
[5]K. J. Kanarik, G. Kamarthy, and R. A. Gottscho, Solid State Technol. **55**(3), 15 (2012).
[6]K. J. Kanarik, S. Tan, J. Holland, A. Eppler, V. Vahedi, and R. A. Gottscho, Solid State Technol. **56**(8), 14 (2013).
[7]E. Pargon, M. Darnon, O. Joubert, T. Chevolleau, L. Vallier, L. Mollard, and T. Lill, J. Vac. Sci. Technol., B **23**, 1913 (2005).
[8]E. Pargon, M. Martin, J. Thiault, O. Joubert, J. Foucher, and T. Lill, J. Vac. Sci. Technol., B **26**, 1011 (2008).
[9]S. A. Vitale, H. Chae, and H. H. Sawin, J. Vac. Sci. Technol., A **19**, 2197 (2001).
[10]W. Jin, S. A. Vitale, and H. H. Sawin, J. Vac. Sci. Technol., A **20**, 2106 (2002).
[11]C. C. Cheng, K. V. Guinn, V. M. Donnelly, and I. P. Herman, J. Vac. Sci. Technol., A **12**, 2630 (1994).
[12]N. Layadi, V. M. Donnelly, and T. C. Lee, J. Appl. Phys. **81**, 6738 (1997).
[13]N. Layadi, V. M. Donnelly, J. T. C. Lee, and F. P. Klemens, J. Vac. Sci. Technol., A **15**, 604 (1997).
[14]K. H. A. Bogart and V. M. Donnelly, J. Appl. Phys. **86**, 1822 (1999).
[15]K. V. Guinn, C. C. Cheng, and V. M. Donnelly, J. Vac. Sci. Technol., B **13**, 214 (1995).
[16]F. H. Bell and O. Joubert, J. Vac. Sci. Technol., B **15**, 88 (1997).
[17]L. Desvoivres, L. Vallier, and O. Joubert, J. Vac. Sci. Technol., B **19**, 420 (2001).
[18]X. Detter, R. Palla, I. Thomas-Boutherin, E. Pargon, G. Cunge, O. Joubert, and L. Vallier, J. Vac. Sci. Technol., B **21**, 2174 (2003).
[19]D. B. Graves and P. Brault, J. Phys. D: Appl. Phys. **42**, 194011 (2009).
[20]H. Feil, J. Dieleman, and B. J. Garrison, J. Appl. Phys. **74**, 1303 (1993).
[21]M. E. Barone and D. B. Graves, J. Appl. Phys. **78**, 6604 (1995).
[22]M. E. Barone and D. B. Graves, Plasma Sources Sci. Technol. **5**, 187 (1996).
[23]D. E. Hanson, A. F. Voter, and J. D. Kress, J. Appl. Phys. **82**, 3552 (1997).
[24]B. A. Helmer and D. B. Graves, J. Vac. Sci. Technol., A **16**, 3502 (1998).
[25]D. E. Hanson, J. D. Kress, and A. F. Voter, J. Chem. Phys. **110**, 5983 (1999).
[26]D. E. Hanson, J. D. Kress, and A. F. Voter, J. Vac. Sci. Technol., A **17**, 1510 (1999).
[27]B. A. Helmer and D. B. Graves, J. Vac. Sci. Technol., A **17**, 2759 (1999).
[28]H. Ohta and S. Hamaguchi, J. Chem. Phys. **115**, 6679 (2001).
[29]H. Ohta and S. Hamaguchi, J. Vac. Sci. Technol., A **19**, 2373 (2001).
[30]D. Humbird and D. B. Graves, J. Chem. Phys. **120**, 2405 (2004).
[31]D. Humbird and D. B. Graves, J. Appl. Phys. **96**, 791 (2004).
[32]F. Gou, E. Neyts, M. Eckert, S. Tinck, and A. Bogaerts, J. Appl. Phys. **107**, 113305 (2010).
[33]A. Iwakawa, H. Ohta, K. Eriguchi, and K. Ono, Jpn. J. Appl. Phys. **47**, 6464 (2008).
[34]A. Iwakawa, T. Nagaoka, H. Ohta, K. Eriguchi, and K. Ono, Jpn. J. Appl. Phys. **47**, 8560 (2008).
[35]H. Ohta, A. Iwakawa, K. Eriguchi, and K. Ono, J. Appl. Phys. **104**, 073302 (2008).
[36]T. Nagaoka, K. Eriguchi, K. Ono, and H. Ohta, J. Appl. Phys. **105**, 023302 (2009).
[37]H. Ohta, T. Nagaoka, K. Eriguchi, and K. Ono, Jpn. J. Appl. Phys. **48**, 020225 (2009).
[38]T. Nagaoka, H. Ohta, K. Eriguchi, and K. Ono, Jpn. J. Appl. Phys. **48**, 070219 (2009).
[39]K. Ono, H. Ohta, and K. Eriguchi, Thin Solid Films **518**, 3461 (2010).
[40]N. Nakazki, Y. Takao, K. Eriguchi, and K. Ono, Jpn. J. Appl. Phys. **53**, 056201 (2014).
[41]H. Tsuda, N. Nakazki, Y. Takao, K. Eriguchi, and K. Ono, J. Vac. Sci. Technol., B **32**, 031212 (2014).
[42]N. Nakazki, H. Tsuda, Y. Takao, K. Eriguchi, and K. Ono, J. Appl. Phys. **116**, 223302 (2014).
[43]H. F. Winters and J. W. Coburn, Surf. Sci. Rep. **14**, 162 (1992).
[44]D. Humbird and D. B. Graves, Plasma Sources Sci. Technol. **13**, 548 (2004).
[45]S. Tinck, E. C. Neyts, and A. Bogaerts, J. Phys. Chem. C **118**, 30315 (2014).
[46]H. D. Hagstrum, Phys. Rev. **122**, 83 (1961).
[47]K. Ono, T. Oomori, M. Tuda, and K. Namba, J. Vac. Sci. Technol., A **10**, 1071 (1992).
[48]K. Ono, M. Tuda, K. Nishikawa, T. Oomori, and K. Namba, Jpn. J. Appl. Phys., Part 1 **33**, 4424 (1994).
[49]M. Tuda and K. Ono, Jpn. J. Appl. Phys., Part 1 **36**, 2482 (1997).
[50]K. Nishikawa, T. Oomori, and K. Ono, J. Vac. Sci. Technol., B **17**, 127 (1999).
[51]F. H. Stillinger and T. A. Weber, Phys. Rev. B **31**, 5262 (1985).
[52]F. H. Stillinger and T. A. Weber, J. Chem. Phys. **88**, 5123 (1988).
[53]F. H. Stillinger and T. A. Weber, Phys. Rev. Lett. **62**, 2144 (1989).
[54]T. A. Weber and F. H. Stillinger, J. Chem. Phys. **92**, 6239 (1990).
[55]H. Sakaue, S. Iseda, K. Asami, J. Yamamoto, M. Hirose, and Y. Horiike, Jpn. J. Appl. Phys. **29**, 2468 (1990).
[56]S. D. Athavale and D. J. Economou, J. Vac. Sci. Technol. A **13**, 966 (1995).
[57]K. J. Kanarik, T. Lill, E. A. Hudson, S. Sriraman, S. Tan, J. Marks, V. Vahedi, and R. A. Gottscho, J. Vac. Sci. Technol., A **33**, 020802 (2015).
[58]H. J. C. Berendsen, J. P. M. Postma, W. F. van Gunsteren, A. DiNola, and J. R. Haak, J. Chem. Phys. **81**, 3684 (1984).
[59]A. W. Kolfschoten, R. A. Haring, A. Haring, and A. E. De Vruies, J. Appl. Phys. **55**, 3813 (1984).
[60]F. H. M. Sanders, A. W. Kolfschoten, J. Dieleman, R. A. Haring, A. Haring, and A. E. de Vries, J. Vac. Sci. Technol., A **2**, 487 (1984).
[61]D. J. Oostra, R. P. van Ingen, A. Haring, and A. E. de Vries, Appl. Phys. Lett. **50**, 1506 (1987).
[62]D. J. Oostra, A. Haring, R. P. van Ingen, and A. E. de Vries, J. Appl. Phys. **64**, 315 (1988).
[63]J. W. Coburn, J. Vac. Sci. Technol., B **12**, 1384 (1994).
[64]M. Balooch, M. Moalem, W.-E. Wang, and A. V. Hamza, J. Vac. Sci. Technol., A **14**, 229 (1996).
[65]J. P. Chang and H. H. Sawin, J. Vac. Sci. Technol., A **15**, 610 (1997).
[66]J. P. Chang and H. H. Sawin, J. Vac. Sci. Technol., B **19**, 1319 (2001).
[67]S. Tachi and S. Okudaira, J. Vac. Sci. Technol., B **4**, 459 (1986).
[68]S. Tachi, K. Tsujimoto, S. Arai, and T. Kure, J. Vac. Sci. Technol., A **9**, 796 (1991).
[69]E. A. Ogryzlo, D. E. Ibbotson, D. L. Flamm, and J. A. Mucha, J. Appl. Phys. **67**, 3115 (1990).
[70]Z. H. Walker and E. A. Ogrtyzo, J. Appl. Phys. **69**, 2635 (1991).
[71]C. Steinbrüchel, Appl. Phys. Lett. **55**, 1960 (1989).
[72]M. Tuda, K. Nishikawa, and K. Ono, J. Appl. Phys. **81**, 960 (1997).
[73]W. Guo and H. H. Sawin, J. Phys. D: Appl. Phys. **42**, 194014 (2009).
[74]A. D. Bailey III, M. C. M. van de Sanden, J. A. Gregus, and R. A. Gottscho, J. Vac. Sci. Technol., B **13**, 92 (1995).
[75]A. D. Bailey III and R. A. Gottscho, Jpn. J. Appl. Phys., Part 1 **34**, 2083 (1995).

[76]C. F. Abrams and D. B. Graves, J. Vac. Sci. Technol., A **16**, 3006 (1998).
[77]V. V. Smirnov, A. V. Stengach, K. G. Gaynullin, V. A. Pavlovsky, S. Rauf, P. J. Stout, and P. L. G. Ventzek, J. Appl. Phys. **97**, 093302 (2005).
[78]V. V. Smirnov, A. V. Stengach, K. G. Gaynullin, V. A. Pavlovsky, S. Rauf, P. J. Stout, and P. L. G. Ventzek, J. Appl. Phys. **97**, 093303 (2005).
[79]V. V. Smirnov, A. V. Stengach, K. G. Gaynullin, V. A. Pavlovsky, S. Rauf, and P. L. G. Ventzek, J. Appl. Phys. **101**, 053307 (2007).
[80]F. O. Goodman and H. Y. Wachman, *Dynamics of Gas-Surface Scattering* (Academic, New York, 1976), Chap. 2, pp. 19−32.
[81]H. Gnaser, *Sputtering by Particle Bombardment: Experiments and Computational Calculations from Threshold to MeV Energies*, Topics in Applied Physics Vol. 110, edited by R. Behrisch and W. Eckstein (Springer, Berlin, 2007), pp. 231–327.
[82]P. Blank and K. Wittmaack, J. Appl. Phys. **50**, 1519 (1979).
[83]J. F. Ziegler, J. P. Biersack, and U. Littmark, *The Stopping and Range of Ions in Matter*, The Stopping and Ranges of Ions in Matter Vol. 1, edited by J. F. Ziegler (Pergamon, New York, 1985), Chap. 2, pp. 14–65.
[84]K. Wittmaack, Phys. Rev. B **68**, 235211 (2003).
[85]G. K. Wehner and D. Rosenberg, J. Appl. Phys. **31**, 177 (1960).
[86]J. Jorzick, J. Lösch, M. Kopnarski, and H. Oechsner, Appl. Phys. A **78**, 655 (2004).
[87]L. H. Bay, J. Bohdansky, W. O. Hofer, and J. Roth, Appl. Phys. **21**, 327 (1980).
[88]M. Stepanova and S. K. Dew, J. Vac. Sci. Technol., A **19**, 2805 (2001).
[89]M. Stepanova and S. K. Dew, Nucl. Instrum. Methods B **215**, 357 (2004).